CALCULATION OF THE THREE DIMENSIONAL PARTICLE TRAJECTORIES IN A TURBINE STAGE

M. Fathy Hussein, et al

Cincinnati University

Prepared for:

Army Research Office

September 1972

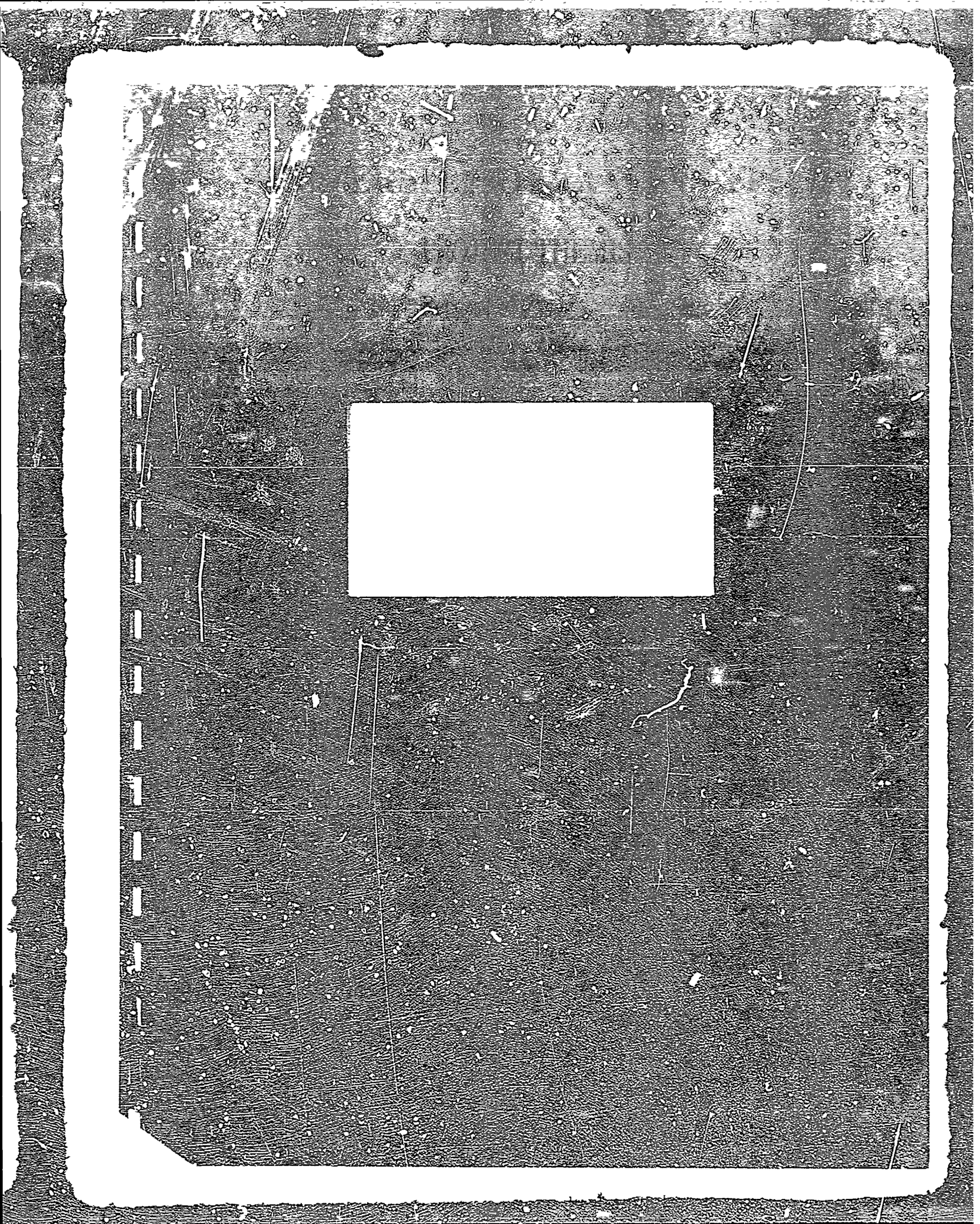

Unclassified
Security Classification

AD 753364

DOCUMENT CONTROL DATA - R & D

(Security classification of title, body of abstract and indexing annotation must be entered when the overall report is classified)

1. ORIGINATING ACTIVITY (Corporate author)
University of Cincinnati

2a. REPORT SECURITY CLASSIFICATION
Unclassified

2b. GROUP
NA

3. REPORT TITLE
Calculation of the Three Dimensional Particle Trajectories in a Turbine Stage

4. DESCRIPTIVE NOTES (Type of report and inclusive dates)
Technical Report

5. AUTHOR(S) (First name, middle initial, last name)
M. Fathy Hussein and W. Tabakoff

6. REPORT DATE
September 1972

7a. TOTAL NO. OF PAGES
~~58~~ 69

7b. NO. OF REFS
27

8a. CONTRACT OR GRANT NO.
DAHC04-69-C-0016

b. PROJECT NO.

c.

d.

9a. ORIGINATOR'S REPORT NUMBER(S)
Project Themis Report No. 27-33

9b. OTHER REPORT NO(S) (Any other numbers that may be assigned this report)

10. DISTRIBUTION STATEMENT
Distribution of this report is unlimited

11. SUPPLEMENTARY NOTES
None

12. SPONSORING MILITARY ACTIVITY
U.S. Army Research Office-Durham
Box CM, Duke Station
Durham, North Carolina 27706

13. ABSTRACT

The equations of motion, in three dimensions, of solid particles entrained by a gas flow through the stationary and rotating cascades of a turbine are derived. The gas velocity components and density at all the mesh points of a square grid constructed in the flow channels are computed assuming a compressible flow. Formulas to determine the proper drag on the particles for a wide range of Reynolds numbers are given. A gas particle flow tunnel is used to investigate experimentally the phenomenon of particle impact with the turbine blades or casing and their rebound from these walls. Formulas for the restitution ratio due to collision and the rebound to incidence angle ratio are derived. This information is used in the equations of motion of the solid particles.

The dynamic behavior of the solid particles in the turbine stage, namely their absolute and relative trajectories, absolute nondimensional velocity history in the channel, and their velocity diagrams as compared to that of the gas, is investigated.

Key Words:

Solid Particulate Flow
Particle Trajectory
Turbomachinery Erosion Phenomena

DD FORM 1473 (PAGE 1) REPLACES DD FORM 1473, 1 JAN 68, WHICH IS OBSOLETE FOR ARMY USE.

Unclassified
Security Classification

AD-753364

PROJECT THEMIS REPORT NO. 72-33

CALCULATION OF THE THREE DIMENSIONAL PARTICLE TRAJECTORIES IN A TURBINE STAGE

M. Fathy Hussein and W. Tabakoff

September 1972

This work was supported by the U.S. Army Research Office - Durham under Project Themis Contract Number DAHC04-69-C-0016

DEPARTMENT OF AEROSPACE ENGINEERING

University of Cincinnati, Cincinnati, Ohio 45221

TABLE OF CONTENTS

LIST OF ILLUSTRATIONS

NOMENCLATURE

α	particle concentration; the ratio between weight flow rate of particles and mixture
β	angle between particle relative velocity and tangent to surface
B	frame fixed in blades (Figure 3)
B_o	origin of B in Figure 3
C_g	absolute gas velocity
C_p	absolute particle velocity
C'_g	gas absolute velocity component in the x,θ plane
C'_p	particles absolute velocity component in the x,θ plane
C_{p_g}	specific heat of gas at constant pressure
Ψ	modified stream function (Equation (47))
$\bar{D}$	drag force on spherical particles
dA	increment of surface area of particle (Equation (16))
d_p	particle mean diameter
Δx	spacing between adjacent points in the meridional direction Figure 14
$\Delta\theta$	spacing between adjacent points in the tangential direction Figure 14
Δt	increment of time
E	frame fixed in the engine (Figure 3)
E_o	origin of E (Figure 3)
$\bar{e}, \bar{e}_1, \bar{e}_2$	unit vectors (Figure 2)
η	angle between relative velocity and meridional plane (Figure 11)
ϕ_1, ϕ_2	coordinate curves in polar coordinates (Figure 2)
ϕ_o	the angle to any vector in the plane $(r, \frac{\pi}{2}, \phi_2)$ (Figure 2)
G	coefficient inversely proportional with the particle characteristics time (Equation (28))

$g(Re)$	Reynolds number dependent function (Equation (6))
h	normal stream channel thickness (blade height) (Figure 4)
$\bar{l}$	unit vector in the direction of blade rotation (Figure 10)
λ	angle between meridional streamline and engine axis (Figure 10)
m_p	mass of one particle (Equation (23))
μ_g	gas viscosity
$\bar{n}_1, \bar{n}_2, \bar{n}_3$	unit vectors in the direction of the coordinate curves x, θ, z
$\bar{N}_1, \bar{N}_2, \bar{N}_3$	unit vectors in the direction of the axes X, Y, Z
0	particle center (Figure 2)
p	pressure at a point
P	total pressure on a spherical particle
R	blade mean radius (Figures 3 and 4)
Re	Reynolds number (Equations (13) and (14))
r	polar coordinate (Figure 2) or radius from axis of rotation (Figure 10)
ρ_g	gas density
$\bar{\rho}_p$	particle material density
s	blade angular spacing
T_g	gas temperature
U	blade speed at the mean radius (Figure 13)
u_g	gas relative velocity component in the x-direction
u_p	particle relative velocity component in the x-direction
V_g	gas relative velocity
V_p	particle relative velocity
V'_g	gas relative velocity component in the x,θ plane
V'_p	particle relative velocity component in the x,θ plane
v_g	gas relative velocity component in the tangential direction
v_p	particle relative velocity component in the tangential direction.

W	weight flow rate of mixture per channel
w_p	particle relative velocity component in the radial direction
ω	blade angular velocity
x,θ,z	coordinate axis in the meridional, tangential and radial direction, fixed in B (Figures 3 and 4)
X,Y,Z	axes fixed in engine (Figures 3 and 4)
$\dot{x},\dot{\theta},\dot{z}$	particle velocity components measured in B
$\ddot{x},\ddot{\theta},\ddot{z}$	particle acceleration components measured in B
$\dot{X},\dot{Y},\dot{Z}$	absolute velocity measured in E
$\ddot{X},\ddot{Y},\ddot{Z}$	absolute acceleration measured in E
y	distance measured along the tangential direction
ξ	outer normal to boundary (Figure 11)

Subscripts

a	absolute trajectory
g	gas
i	initial conditions at particles entrance
in	conditions at the boundary AH (Figure 14)
n	normal to surface
o	total conditions
out	after cascade
p	particle
t	tangent to surface
x	in the x-direction
y	in the y-direction
z	in the z-direction
1	before collision
2	after collision

ABSTRACT

The equations of motion, in three dimensions, of solid particles entrained by a gas flow through the stationary and rotating cascades of a turbine are derived. The gas velocity components and density at all the mesh points of a square grid constructed in the flow channels are computed assuming a compressible flow. Formulas to determine the proper drag on the particles for a wide range of Reynolds numbers are given. A gas particle flow tunnel is used to investigate experimentally the phenomenon of particle impact with the turbine blades or casing and their rebound from these walls. Formulas for the restitution ratio due to collision and the rebound to incidence angle ratio are derived. This information is used in the equations of motion of the solid particles.

The dynamic behavior of the solid particles in the turbine stage, namely their absolute and relative trajectories, absolute nondimensional velocity history in the channel, and their velocity diagrams as compared to that of the gas, is investigated. The effect of different flow parameters, mainly, the particle mean diameter, material density, and particle and gas initial velocities on the dynamic characteristics of the solid particles are studied.

Observations concerning the erosion damage suffered by the turbine stator and rotor blades as well as the turbine casing due to the solid particle impingements are presented.

INTRODUCTION

Rockets, aircraft engines, and industrial gas turbines operating in desert or dusty areas and in places where the atmosphere is polluted by small solid particles from factories and car exhausts can be examples of machines operating under gas particle two phase flow conditions. Another example is engines that burn fuels which produce solid particles in the products of combustion. The solid particles mixed with the inlet air or combustion gases, due to the difference in their inertia, will be driven away from the streamlines of the gas and impact with the surrounding walls of the engine. The presence of solid particles in the gas stream constitute a possible cause for severe erosion damage to the engine parts. The erosion damage caused by solid particles is expected to be more severe in the rotating parts of the engine, where the particle velocities and frequency of impacts, as well as the flow temperature, are higher. Hence, turbines, axial or centrifugal, of rockets or gas turbines are parts of the engine critically subjected to solid particle erosion. For example, in some instances the life of a turbine of a helicopter engine is decreased by one-fourth due to its operation in a solid particle suspension as compared to engines operating under normal conditions. This gives an indication to the seriousness of the problem from the economical and reliability points of view. The rate of erosion damage to the blades of the stator or the rotor of turbines is a function of the blade and particle materials, the gas conditions in the channel, the angle of impact of the solid particles with the blade surface, the velocity of impact and the frequency of collisions. In rotating turbomachinery the centrifugal forces acting on the particles, due to its motion in a circular path, tends to force the solid particles to move radially, and hence, impact with the turbine casing, causing it to also suffer from erosion damage. Furthermore, the rebound of the particles from the casing wall will increase the frequency of collisions with the blades. This discussion points out the fact that the solid particles motion in a rotating turbomachine is a three-dimensional problem.

In order to further understand the erosion phenomenon of rotating turbomachines, it is important to study the dynamic characteristics or behavior of the solid particles entrained by the gas flow through the stages of turbines. By the dynamic behavior, it is meant, the absolute and relative position of the solid particles everywhere in the channels, the velocity history and velocity diagrams of the particles as well as a description of the collision and rebound mechanisms of the solid particles from the blade and casing walls. The particles trajectories studied in rotating turbomachinery furnishes information for correlating experimentally determined erosion severity of blades and the characteristics of particle impact on surfaces. It also helps to predict the erosion of proposed cascade designs based on the correlation results and thus initiate means to protect blades and walls by minimizing erosion damage. In fact, the investigation of the solid particles dynamic behavior will enable engineers to design turbines and compressors to minimize erosion as well as to optimize aerodynamic characteristics.

This investigation was devoted to studying the dynamic behavior of

solid particles in a turbine stage. The effect of different flow parameters such as particle mean diameter, material density and initial particle and gas velocities on the particle dynamic behavior are investigated. Results of this study are then used to make observations concerning the areas of the blades or casing that are subjected to more impacts and hence, higher rates of erosion damage.

The three-dimensional equations of motion of solid particles moving in a compressible gas stream in a rotating cascade of a turbomachine are derived in a general form. They are solved to determine the particle trajectories and velocities in an axial or radial rotating turbomachinery or any similar three or two-dimensional particulate flow problem as special cases. In order to derive and solve the equations of motion in the three-dimensional space of solid particles, several assumptions concerning the analysis have to be made. Also bassic information about the impact and rebound phenomenon, drag on particles, and gas properties has to be investigated.

It is assumed that the particles enter the stator of the turbine or compressor with uniform properties and equal distances apart. The particles are assumed to be spheres of constant average mean diameter uniform material density and small in size. The forces acting on the solid particles causing their motion in the flow are assumed to be mainly the drag forces exerted on them by the gas. It is further assumed that the presence of solid particles does not alter the gas properties from that for the case of gas flow alone passing through the same cascade. This assumption is more realistic for higher particle material densities and small particle concentrations. The particle concentration α, is defined by the ratio of mass flow rate of particle to the rate of mass flow of the mixture. Higher material densities implies smaller number of particles for the same concentration.

After particles impact with the blade or casing, they suffer a drop in their velocities and a change in their direction. In order to study the impact and rebound phenomenon, a simple test facility is designed, where particles and blades of the same materials as in actual operating conditions are used. Particles are injected into the flow in the test section and photographed by a high-speed camera. Analysis of the high-speed photography of the collision phenomenon gives the restitution ratio and the ratio of the rebound to the incidence angle as a function of the incidence angle. These two ratios, or any equivalent ratios, are sufficient to define the mechanism of impact for a certain particle-wall material combination. From these ratios, the relative velocity and the direction of motion of the particle after collision are computed and used as the initial conditions to the solution of the governing equations of motion for the particles.

The drag coefficient on spherical particles has to be known for the practical range of the Reynolds numbers based on particle mean diameter and the magnitude of the difference in gas and particle velocities. Analytical relations to determine the drag coefficient as a function of the Reynolds number may be derived from the solution of the Navier-Stokes equations, which are valid for Reynolds numbers up to 4. Empirical formulas that fit the experimental results for the drag coefficient on spheres moving in a stream of air are derived up

to the practical limit of the Reynolds number of such types of flows. These formulas permit accurate calculations of the drag forces acting on the particle and increase the range of application of the equations of motion of solid particles.

The remaining information that has to be known before solving the particle equations of motion are the gas properties, mainly its density and velocity components everywhere in the channel. The equations of motion of a compressible gas moving in a rotating cascade are solved. A square grid is constructed in the channel and the gas properties are calculated at all mesh points. The gas properties anywhere in the nozzle could then be interpolated. The gas properties are calculated at all mesh points in every row of blades and stored on computer magnetic tape in groups of data each representing a cascade row that constitutes the stages of the turbine.

The equations of motion of the particles are formulated with respect to axes fixed in the blades at the entrance of the cascade row. With the impact phenomenon well described, and the drag coefficient and gas properties known, the equations of motion of the particles are solved. One row of blades is considered at a time, the particles enter the row with known initial conditions, hit the walls and rebound (several rebounds may occur) until they leave the nozzle. The particles outlet conditions constitute the initial condition for the successive row. The equations of motion of particles with respect to a new frame of axes using the known initial conditions are solved using the corresponding gas conditions in the new cascade row and so on. The particles positions are referred to the initial axes by a simple transformation. Repeated solution of the equations of motion of the particles for all successive cascade rows gives the particles dynamic behavior throughout the turbine. The absolute trajectories of the particles show its real path, while the relative trajectories indicate its path relative to the rotor. This information can be used to determine the erosion rate, knowing the momentum loss due to impacts and their frequency at a certain area. The particles velocity diagrams as compared to the gas velocity diagram of a stage would illustrate the general behavior of the particles and their deviations from the gas at inlet and exit ports.

The study of particles trajectories in flow fields such as nozzles, pipes and cyclones are reported in many articles (References 1-5). However, none of these investigations solve the three-dimensional problem, or take the collision of particles with the walls or the rotating cascade type problem into consideration. In References 6, 7, and 8 experimental and theoretical studies are made by the author, to study or simulate the dynamic behavior of solid particles. The results of the two-dimensional experimental study of Reference 6, the theoretical study of Reference 8 and the results of this investigation seem to agree with the physical observation of eroded cascades of tested and real engines. The results of this investigation provide an understanding of the behavior of the particles in the rotors, a contribution that was difficult to accomplish by the simulation of Reference 7. The computer program used in the study is given by the authors in Reference 9. It can be used with slight modifications to calculate particle trajectories and velocities in two or three dimensions, stationary or rotating axial or radial turbomachinery.

FORCES ON SPHERICAL PARTICLES MOVING IN A GAS STREAM

The forces that act on solid spherical particles suspended by the gas flow are the drag force, the force due to the pressure gradient in the fluid surrounding the particles, the force to accelerate the apparent mass of the particle relative to the fluid, the Magnus force, and the Basset force that takes into account the deviation in the flow pattern from steady state, see Reference 10. Newton's law of motion may be used to describe the particle motion, where the sum of the forces acting on the particle plus its inertia force vanishes. The force on a small particle suspended in a turbulent flow is given in Reference 11. Further discussions of the problem are reported in References 12, 13 and 14. It is assumed that the particles are spherical in shape, so that the drag force may be calculated using the Stokes drag coefficient, however, correction to the value of the drag forces at higher Reynolds number is introduced. It is further assumed that the particles are small when compared to the smallest wave length of the turbulence, hence the effect of particle motion due to shear flow is neglected. Since in the case of particulate flow problems in gas turbines, the particle mean diameter is small and the density of particle material is much higher in magnitude than the gas density, the force due to pressure gradient, the force to accelerate the apparent mass of the particles and the Basset force may be neglected compared to drag force (Reference 10). The drag force and force due to pressure gradient acting on a spherical particle are discussed herein, however, the equations of motion for the particles are solved taking only the drag force into account.

Drag Force

An analytical solution of the governing equations of motion for a gas flow around a spherical particle is available only for very slow moving particles, i.e. for small Reynolds number.

To determine the drag force acting on the solid particles, consider the motion of a spherical particle in a steady, slow moving, incompressible gas flow. If the inertia forces can be neglected compared to the viscous forces, and for no body forces, the Navier-Stokes equations become;

$$\text{grad } p = \mu_g \nabla^2 (\bar{C}_g) \tag{1}$$

The continuity equation of the gas may be written as

$$\text{Div } (\bar{C}_g) = 0 \tag{2}$$

The solution of Equations (1) and (2) (References 8 and 15) yields the total drag force acting on the spherical particles for Reynolds number less than 0.1 as;

$$\bar{D} = 3 \pi \mu_g d_p \bar{C}_g \tag{3}$$

If the particle is moving with an absolute velocity $\bar{C}_p$ in a stream of gas moving with an absolute velocity $\bar{C}_g$, the drag force on the spherical

particle may be written as;

$$\bar{D} = 3 \pi \mu_g d_p (\bar{C}_g - \bar{C}_p) \tag{4}$$

For higher Reynolds numbers, Equation (4) connot be considered valid, a correction factor for this equation which is a function of the Reynolds number was introduced (References 8 and 15).

The modified version of Equation (4) may take the form,

$$\bar{D} = 3 \pi \mu_g d_p (\bar{C}_g - \bar{C}_p) \, g(Re) \tag{5}$$

where

$$g(Re) = C_D \frac{Re}{24} = \frac{C_D}{C_{D_o}} \tag{6}$$

In Equation (5) the Reynolds number dependent function g(Re) has different forms depending on the range of the Reynolds number. It should have a value of one for Reynolds numbers less than 1.0. Its value can be determined theoretically from the solution of the Navier-Stokes equations for Reynolds numbers up to 4. The experimental data for drag coefficients on a sphere has to be used to determine g(Re) for Reynolds numbers greater than 4 and within the practical limit of Reynolds number for particulate gas flow in turbomachines. Equation (6) shows that the function g(Re) can be given as a ratio between the drag coefficient at any Reynolds number and the Stokes drag coefficient at small Reynolds number.

The formulas for the drag coefficient for spherical particles as defined in Equation (6) are given below for different ranges of the Reynolds number.

$$C_D = \frac{24}{Re} \qquad 0 < Re \leq 1.0 \tag{7}$$

A solution of the Navier-Stokes equations of motion of a solid particle using a higher order term gives,

$$C_D = \frac{24}{Re} \left(1 + \frac{3}{16} Re\right) \qquad 1.0 < Re \leq 4.0 \tag{8}$$

The experimental data given by Schlichting (Reference 16) for the drag coefficient of spherical particles are fitted (Reference 17) with a curve of the type

$$y = a x^b + \alpha \tag{9}$$

where

$$\alpha = \frac{y_1 y_2 - y_3^2}{y_1 + y_2 - 2y_3} \tag{10}$$

The resulting drag coefficient formula is given by

$$C_D = 21.9416\ Re^{-0.718} + 0.3240 \qquad 4.0 < Re \leq 2000 \tag{11}$$

For higher Reynolds number one may write,

$$C_D = 0.4 \qquad Re > 2000 \tag{12}$$

The Reynolds number in Equations (7), (8), (11) and (12) is based on the particle mean diameter and the magnitude of the particle velocity relative to the gas or,

$$Re = \frac{d_p\ \rho_g}{\mu_g} \left|(\bar{V}_g - \bar{V}_p)\right| = \frac{d_p\ \rho_g}{\mu_g} \left|(\bar{C}_g - \bar{C}_p)\right| \tag{13}$$

or

$$Re = \frac{d_p\ \rho_g}{\mu_g} \sqrt{(u_g - \dot{x})^2 + (v_g - \dot{y})^2 + (w_g - \dot{z})^2} \tag{14}$$

Figure 1 gives the fitted drag curve as compared to the experimental results and it shows good agreement.

Force Due to Pressure Gradient in the Flow Around the Particle

In order to evaluate the force acting on a spherical particle due to the pressure gradient around it, consider a spherical particle of diameter d_p and center 0 in a flow field (Figure 2). The pressure at any point on the particle surface is $p(d_p/2, \phi_1, \phi_2)$ and the pressure at 0 is p_o. The polar coordinates r, ϕ_1 and ϕ_2 originate from the sphere's center. The coordinate ϕ_1 is measured from the direction of the gradient vector of the pressure at the center $(\nabla p)_o$. The vector $\bar{e}$ is a unit vector from the center of the sphere to any point $p(d_p/2, \phi_1, \phi_2)$. Also $\bar{e}_1$ and $\bar{e}_2$ are the unit vectors in the direction of $(\nabla p)_o$ and any normal to it that makes an angle $(\phi_2 - \phi_o)$ from the projection of $\bar{e}$ on the plane $\phi_1 = \pi/2$.

The pressure $p(d_p/2, \phi_1, \phi_2)$ at any point on the surface of the sphere is given by

$$p \equiv p\left(\frac{d_p}{2}, \phi_1, \phi_2\right) = p_o + \frac{\partial p}{\partial \bar{e}} \cdot \frac{d_p}{2}$$

$$= p_o + \frac{d_p}{2} \left[(\nabla p)_o \cdot \bar{e}\right]$$

or

$$p = p_o + \frac{d_p}{2} |(\nabla p)_o| \cos \phi_1 \cdot \tag{15}$$

The total force acting on the particle, $\bar{P}$, equals the sum of these pressure forces on the surface of the sphere, i.e.

$$\bar{P} = \int (p\ \bar{e})\ dA \tag{16}$$

where dA is the increment of area of the surface of the sphere whose normal is $\bar{e}$. Using Equation (15), Equation (16) may be rewritten as

$$\bar{P} = \frac{d^3_p}{8} |(\nabla p)_o| \int_o^{2\pi} \int_o^{\pi} \bar{e} \sin \phi_1 \cos \phi_1\ (d\ \phi_1)(d\ \phi_2) \tag{17}$$

The component of $\bar{P}$ in the $\bar{e}_1$ direction is $\bar{P}_1$ given by

$$\bar{P}_1 = \frac{d^3_p}{8} |(\nabla p)_o| \int_o^{2\pi} \int_o^{\pi} \sin \phi_1 \cos^2 \phi_1\ (d\ \phi_1)(d\ \phi_2)$$

or

$$\bar{P}_1 = \frac{\pi\ d^3_p}{6} |(\nabla p)_o| \tag{18}$$

The component of $\bar{P}$ in any direction $\bar{e}_2$ perpendicular to $\bar{P}_1$ is $\bar{P}_2$ and may be given by

$$\bar{P}_2 = \frac{d^3_p}{8} |(\nabla p)_o| \int_o^{2} \cos (\phi_2 - \phi_o)(d\ \phi_2) \cdot$$

$$\cdot \int_o^{\pi} \sin^2 \phi_1 \cos \phi_1\ (d\ \phi_1) = 0 \tag{19}$$

Since $\bar{P}_2$ vanishes for any arbitrary direction $\bar{e}_2$, the force $\bar{P}$ is then in the direction of $\bar{e}_1$, i.e., the direction of the vector $(\nabla p)_o$ and is given by

$$\bar{P} = \int (p\ \bar{e})\ dA = \frac{\pi\ d^3_p}{6} (\nabla p)_o$$

$$= \frac{m_p}{\rho_p} (\nabla p)_o \tag{20}$$

where m_p and $(m_p/\bar{\rho}_p)$ are the mass and volume of one particle, respectively.

Using Euler's equation of motion for the gas, the force P, acting on the particle due to the pressure gradient may be written as

$$\bar{P} = \left(\frac{m_p}{\bar{\rho}_p}\right)(\nabla p)_o = m_p \left(\frac{\rho_g}{\bar{\rho}_p}\right)(\bar{C}_g \nabla)\, \bar{C}_g \qquad (21)$$

EQUATIONS OF MOTION OF SOLID PARTICLES ENTRAINED BY THE GAS FLOW IN A ROTATING CASCADE

The turbine may be divided into separate successive rows, for example, stator, rotor, stator, etc. The particles are assumed to enter the first row with their initial conditions referred to a system of axes associated with the first row. The conditions of the particles at the outlet of the first row may be transformed to another set of axes associated with the second row of blades, stationary or rotating, and these will be considered initial conditions for the second cascade row and so on, until the particles leave the turbine with the conditions at the exit of the last cascade row. In order to derive the equations of motion of the particles suspended by the gas flow, their motion through a rotating cascade row is considered, with the case of particle motion in a stator blade row, following as a special case. It is convenient to define systems of axes associated with each cascade row to simplify the computer programming problems, as well as yielding a simpler set of equations of motion for particles in the rotor blades.

For convenience, the following axes systems are defined. B is a frame fixed in an arbitrary blade of the rotating cascade with $\bar{n}_1$, $\bar{n}_2$ and $\bar{n}_3$ as a set of nonparallel, noncoplaner, right-handed unit vectors in the direction of the coordinate curves x, θ and z, respectively, as shown in Figure 3 and 4. The point B_o is the origin of the frame B, which is taken at the intersection of the plane tangent to the blade row at the entrance and the blade axial chord in the mid-stream surface of revolution of radius R that passes through the middle of the blade height. The coordinate curves x, θ and z are in the axial or meridional direction, the tangential, and the radial directions, respectively. Further, it is assumed that the frame B, fixed in the blade row, moves with a constant angular velocity ω, equal to the angular speed of the rotor, in a reference frame E fixed in the engine. The mutually perpendicular set of axes X, Y and Z, are fixed in the engine at a point E_o. Point E_o is the intersection of the engine axis with the plane tangent to the blade row at the entrance. The coordinate axis X is in the axial direction, while Y and Z are axes normal to the X axis in the plane tangent to the blade row at the entrance, as shown in Figures 3 and 4.

Consider the motion of a solid particle entrained by the gas flow past a rotating cascade. Referring to Figure 5, the coordinate curves x, θ and z, that rotate with an angular velocity ω, after a time t, are at an angle equal to ωt from the Z axis. The particle p is at any

arbitrary position x, θ and z measured from B_o.

According to Newton's law of motion the forces acting on the particle, taken to be the drag force, equals the mass of the particle multiplied by its acceleration in an inertial reference frame. The equations of motion of the particle p with respect to the axes X, Y and Z of the fixed reference frame E are

$$m_p \ddot{X}_p = D_X$$

$$m_p \ddot{Y}_p = D_Y$$

$$m_p \ddot{Z}_p = D_Z \tag{22}$$

where m_p is the mass of one particle given by

$$m_p = \frac{1}{6} \pi d_p^3 \bar{\rho}_p \tag{23}$$

and $\ddot{X}_p$, $\ddot{Y}_p$ and $\ddot{Z}_p$ are the second derivatives with respect to time of the components of the position vector of p in E.

From Equation (5) the components of the drag force in the reference frame E, as given in Equation (22) are written as

$$D_X = 3 \pi \mu_g d_p g(Re) (\dot{X}_g - \dot{X}_p)$$

$$D_Y = 3 \pi \mu_g d_p g(Re) (\dot{Y}_g - \dot{Y}_p)$$

$$D_Z = 3 \pi \mu_g d_p g(Re) (\dot{Z}_g - \dot{Z}_p) \tag{24}$$

In Equation (24) $\dot{X}_g$, $\dot{Y}_g$ and $\dot{Z}_g$ are the gas velocity components at p in E, while $\dot{X}_p$, $\dot{Y}_p$ and $\dot{Z}_p$ are the velocity components of a particle at p in E.

Substituting Equations (23) and (24) into Equation (22) we get

$$\ddot{X}_p = G(\dot{X}_g - \dot{X}_p) \tag{25}$$

$$\ddot{Y}_p = G(\dot{Y}_g - \dot{Y}_p) \tag{26}$$

$$\ddot{Z}_p = G(\dot{Z}_g - \dot{Z}_p) \tag{27}$$

where

$$G = \frac{18\ \mu_g}{d_p^2\ \bar{\rho}_p}\ g(Re) \tag{28}$$

The coefficient G is a measure of the particle characteristic time which indicates the relaxation time of the particles relative to the gas flow.

From Figure 5, the relation between the components of the position vector and its first and second derivatives with respect to time measured from E_o and the components of the position vector and its time derivatives measured from B_o of the particle p, is given by

$$X = x \qquad \dot{X} = \dot{x} \qquad \ddot{X} = \ddot{x} \tag{29}$$

$$\begin{aligned} Y &= (R + z)\sin(\theta + \omega t) \\ \dot{Y} &= \dot{z}\sin(\theta + \omega t) + (R + z)(\dot{\theta} + \omega)\cos(\theta + \omega t) \\ \ddot{Y} &= \ddot{z}\sin(\theta + \omega t) + 2\dot{z}(\dot{\theta} + \omega)\cos(\theta + \omega t) \\ &\quad + (R + z)\left[-(\dot{\theta} + \omega)^2 \sin(\theta + \omega t) + \ddot{\theta}\cos(\theta + \omega t)\right] \end{aligned} \tag{30}$$

$$\begin{aligned} Z &= (R + z)\cos(\theta + \omega t) \\ \dot{Z} &= \dot{z}\cos(\theta + \omega t) - (R + z)(\dot{\theta} + \omega)\sin(\theta + \omega t) \\ \ddot{Z} &= \ddot{z}\cos(\theta + \omega t) - 2\dot{z}(\dot{\theta} + \omega)\sin(\theta + \omega t) \\ &\quad - (R + z)\left[(\dot{\theta} + \omega)^2 \cos(\theta + \omega t) + \ddot{\theta}\sin(\theta + \omega t)\right] \end{aligned} \tag{31}$$

The velocity components of the gas at any point p with reference to E_o, neglecting the gas velocity in the radial direction compared to the gas velocity in the axial and tangential directions, are written as,

$$\begin{aligned} \dot{X}_g &= u_g \\ \dot{Y}_g &= [v_g + (R + z)\omega]\cos(\theta + \omega t) \\ \dot{Z}_g &= [v_g + (R + z)\omega]\sin(\theta + \omega t) \end{aligned} \tag{32}$$

where u_g and v_g are the components of gas velocity relative to the rotating blades in the axial and tangential directions, respectively.

Substituting Equations (29), (30), (31) and (32) in Equations (25),

(26) and (27), find

$$\ddot{x} = G\,(u_g - \dot{x}) \tag{33}$$

$$\ddot{z}\sin(\theta + \omega t) + 2\dot{z}(\dot{\theta} + \omega)\cos(\theta + \omega t) - (R + z)[(\dot{\theta} + \omega)^2 \sin(\theta + \omega t) + \ddot{\theta}\cos(\theta + \omega t)] = G\{[v_g + (R + z)\omega]\cos(\theta + \omega t) - \dot{z}\sin(\theta + \omega t) - (R + z)(\dot{\theta} + \omega)\cos(\theta + \omega t)\} \tag{34}$$

$$\ddot{z}\cos(\theta + \omega t) - 2\dot{z}(\dot{\theta} + \omega)\sin(\theta + \omega t) - (R + z)[(\dot{\theta} + \omega)^2 \cos(\theta + \omega t) + \ddot{\theta}\sin(\theta + \omega t)] = G\{[v_g + (R + z)\omega]\sin(\theta + \omega t) - \dot{z}\cos(\theta + \omega t) + (R + z)(\dot{\theta} + \omega)\sin(\theta + \omega t)\} \tag{35}$$

Multiplying Equation (34) by cos $(\theta + \omega t)$, Equation (35) by sin $(\theta + \omega t)$, and subtracting the two resulting equations and rearranging, we get the equation of motion of the particle p in the tangential direction as

$$(R + z)\ddot{\theta} = G[v_g - (R + z)\dot{\theta}] - 2\dot{z}(\dot{\theta} + \omega). \tag{36}$$

Multiplying Equation (34) by sin $(\theta + \omega t)$, Equation (35) by cos $(\theta + \omega t)$, and adding the two resulting equations and rearranging, we get the equation of motion of the particle p in the radial direction as

$$\ddot{z} = -G\dot{z} + (R + z)(\dot{\theta} + \omega)^2 . \tag{37}$$

The distance y that a particle travels in the θ direction on the surface of revolution with radius $(R + z)$ is given by

$$y = (R + z)\,\theta \tag{38}$$

For convenience Equations (33), (36) and (37) may be rewriteen as

$$\ddot{x} = G\,(u_g - \dot{x}) \tag{39}$$

$$\ddot{\theta} = \frac{G}{(R + z)}[v_g - (R + z)\dot{\theta}] - \frac{2\dot{z}}{(R + z)}(\dot{\theta} + \omega) \tag{40}$$

$$\ddot{z} = -G\dot{z} + (R + z)(\dot{\theta} + \omega)^2 \tag{41}$$

Re and G are given by Equations (14) and (28), respectively.

Equations (39), (40) and (41) are the governing equations of motion of any particle p moving with the gas stream through the nozzles of a rotating cascade. They represent the equations of motion in the axial, tangential and radial directions, respectively. The coordinate curves x, θ and z measured in the frame of axes B and their first and second time derivatives as well as the relative gas velocity components in the axial and tangential directions are taken at the particular point under consideration. It is noted that the second term in the right hand side of Equation (40) represents Coriolis acceleration, while the second term in the right hand side of Equation (41) represents the centrifugal accelerations of a particle moving in curved path in the rotating frame B. (References 18 and 19). These equations form a system of nonlinear differential equations. They are solved numerically for every particle entering the cascade in increments of time if the initial conditions of the particle are known. The time increment may have a constant value as long as it does not take the particle beyond the wall, thus, at the regular increment nearest the wall, the time increment has to be iterated to the exact value that is necessary for the particle to just hit the wall. Solution of the general system of equations of the type of Equations (39), (40) and (41) and a discussion of the error are given in Reference 9. The solution of the particle equations of motion gives the relative and absolute locations as well as the velocity components of a particle in the rotating cascade row. Successive solution of these equations for every cascade row will give the particles path throughout the turbine. The solution of these equations requires the knowledge of the coefficient G, the collision and rebound mechanism of the particles and the turbine walls as well as the gas properties in the channel.

EXPERIMENTAL STUDY OF THE IMPACT AND REBOUND PHENOMENON OF SOLID PARTICLES FROM THE WALLS

When a solid particle moves in a stream of gas, it does not in general follow the streamlines taken by the gas due to its higher inertia. For particulate gas flow passing through the nozzles of a rotating cascade, the particles tend to collide with the blade surfaces. They often collide with the turbine casing due to the effect of the centrifugal force acting on the particle. After hitting the walls, the particles experience a loss in their momentum relative to the wall and change the direction of their motion. They may hit the blades one or more times before leaving the cascade. These repeated collisions of several particles causes severe erosion damage to the blades. The analytical study of the impact phenomenon of particles with a rotating blade in three dimensions is a very difficult task. The value of the particle velocity and direction of its motion as it rebounds from the surface after collision must be known in order that the solution of the particle equations of motion be continued beyond the points of collision. In order to investigate the collision phenomenon, an experimental study was made, where the particles were photographed and their behavior during this process is studied. The experimental facilities of Reference 15 were used and extensive results for steel blades and corn cups particles

have been collected and analysed so as to determine the behavior of solid particles before and after the collision with the walls. The result of this study is given in details in References 8 and 15 and may be summarized as follows.

The change in particle momentum due to collisions was found to be mainly a function of the particle incidence angle β_1. In Figure 6, the ratio of the particle velocity tangent to the surface after and before collision ($V_{p_{t2}}/V_{p_{t1}}$) is plotted versus β_1, and may be considered constant for all particle diameters. The dotted line in Figure 6 represents the straight line fitting the experimental data expressed by the equation,

$$V_{p_{t2}} / V_{p_{t1}} = 0.95 + 0.00055\ \beta_1 \tag{42}$$

The change in the ratio between particle velocity components normal to the surface of the blade after and before collision ($V_{p_{n2}}/V_{p_{n1}}$), as a function of β_1, is given in Figure 7 for different particle diameters. The dotted curve in Figure 7 represents the curve fitting of the data points on the figure expressed by the following relation

$$\frac{V_{p_{n2}}}{V_{p_{n1}}} = 1.0 - 0.002108\ \beta_1 + 0.0001417\ \beta_1^2 \tag{43}$$

The restitution ratio (V_{p_2}/V_{p_1}) is defined as the ratio between the particle velocities after and before collision. Another important factor is the rebound to incidence angle ratio (β_2/β_1), defined as the ratio of the angle between the direction of the incidence particle velocity and the tangent to the surface at the point of impact and the angle between the direction of the rebound particle velocity and the tangent to the surface at the same point.

Figure 8 gives β_2/β_1 as a function of β_1. The dotted curve is obtained by substituting Equations (42) and (43) into the following relation.

$$\frac{\beta_2}{\beta_1} = \frac{1}{\beta_1} \cot^{-1} \left[\left(\frac{V_{p_{t2}}}{V_{p_{t1}}} \cdot \frac{V_{p_{n1}}}{V_{p_{n2}}}\right) \cdot \cot \beta_1\right] \tag{44}$$

In Figure 9, the restitution ratio is presented versus β_1. Equations (42) and (43) together with the following equation are used to plot the dotted curve in the figure.

$$\frac{V_{p_2}}{V_{p_1}} = \frac{V_{p_{n2}}}{V_{p_{n1}}} \cdot \sqrt{\frac{1 + \cot^2 \beta_2}{1 + \cot^2 \beta_1}} \tag{45}$$

Once the particles and blade materials are known for a certain gas turbine application, fundamental experiments can be conducted to render information about the impact and rebound phenomenon of this particular material combination. It may be added that in order to simplify the analysis the formulas found to describe the impact phenomenon do not take into account any deposits or wear that may be suffered by the blade material due to collisions. Either Equations (42) and (43) or Equations (44) and (45) are enough to define the particle condition just after rebound from the surface. They give new initial conditions to be used in the solution of the equations of motion of the particles after collision.

GAS FLOW PROPERTIES IN A BLADE TO BLADE SURFACE OF REVOLUTION OF A ROTATING CASCADE

The assumption that the gas flow moves in the blade to blade surface of revolution shown in Figure 10, is applicable to axial or radial flow cascades. The coordinate curves x, θ and z are fixed in the blade as described earlier, in general they are in the meridional direction, tangential and normal to the blade to blade surface of revolution. It is required to determine the properties of the compressible gas flow, namely the gas density, ρ_g, and the velocity components in the meridional and tangential direction, u_g and v_g, in both the rotating channels of the cascade and on the blades. A solution to the momentum, continuity, energy and state equations that conveniently describe the gas flow in a rotating cascade provide the gas properties required in the solution of the governing equations of motion of the particles. For small particle concentrations it can be assumed that the gas conditions calculated from the solution of the nonparticulate gas flow equations of motion in a rotating turbomachine are not going to be altered due to the presence of particles in the flow.

For a compressible, nonviscous and steady gas flow, the momentum and continuity equations (References 15 and 20) may be written as,

$$\frac{\partial^2\Psi}{\partial x^2} + \frac{1}{r^2}\frac{\partial^2\Psi}{\partial\theta^2} + \left[\frac{\sin\lambda}{r} - \frac{1}{h\,\rho_g}\frac{\partial(h\,\rho_g)}{\partial x}\right]\frac{\partial\Psi}{\partial x}$$

$$- \frac{1}{r^2\rho_g}\frac{\partial\rho_g}{\partial\theta}\frac{\partial\Psi}{\partial\theta} = \frac{2\,h\,\rho_g}{W}\,\omega\,\sin\lambda \qquad (46)$$

where

$$u_g = \frac{W}{rh\,\rho_g}\frac{\partial\Psi}{\partial\theta}$$

$$v_g = -\frac{W}{h\,\rho_g}\frac{\partial\Psi}{\partial x} \qquad (47)$$

and

Ψ is the modified version of the stream function.

The combined energy and state equation is

$$\frac{\rho_g}{\rho_{g_{in}}} = \left[1 - \left(\frac{|\bar{C}_g|^2}{2\, C_{p_g}\, T_{g_{in}}}\right)\right]^{\frac{1}{\gamma-1}} \qquad (48)$$

The turbine cascade channel region ABCDEFGH in Figure 11 is divided into square grids, the difference equation (Reference 9) of Equation (46) is written at all the mesh points. A solution by the method of over-relaxation (Reference 21) to the n resulting algebraic equations is obtained using assumed initial values for the gas density, say the absolute total density at inlet. The solution of these equations gives the modified stream function at the mesh points. The approximate relative gas velocity components at all the mesh points are then calculated from Equations (47). Equation (48) may then be used to compute new gas densities at the mesh points. These new densities are used to determine a better approximation for the modified stream function and hence the relative gas velocity, which are then used to determine new gas densities and so on, until the required accuracy in calculating the gas density is reached. The fortran program Reference 22 is modified slightly to give the relative gas velocity components and densities at the mesh points, by solving Equations (46) and (48) then store the data for a cascade row on magnetic tape, to be used as data in the solution of the particle equations of motion. Other methods to determine the gas properties in the cascade by placing singularities on the contour of the airfoil (Reference 23), or by distributing the singularities on the camber and chord lines (Reference 24) may be used. The gas flow in these cases is considered incompressible and correction for the compressibility effect has to be introduced (Reference 25). Another method (Reference 26) gives the compressible gas flow properties for a subsonic cascade flow by the method of distributing vorticities along the blade contour. The advantage of using a square grid is that it may be used as a means to specify the particle location in the channel. The decision on which method to use to determine the gas properties should be a compromise between accuracy, range of application and computer time.

NUMERICAL EXAMPLE

The dynamic characteristics of particles entrained by a gas through a turbine stage consisting of a stator followed by a rotor is considered herein. The effect of different particle and gas flow parameters on the particle characteristics are investigated. The parameters considered are the particles mean diameter, their material density and their initial nondimensional absolute velocity, as well as the gas velocity at the inlet. The particle trajectories and velocities are calculated from Equations (38), (40) and (41). The drag coefficient

is calculated using Equations (7), (8), (11) and (12), the impact and rebound characteristics from Equations (44) and (45), and the gas properties in the cascade are obtained by solving Equations (46) and (48). The computer program described in Reference 9 is used on the IBM 360 computer, and the output punched on cards. These cards are fed as an input to the Calcomp plotter which is programmed through the IBM 1130 computer to plot the trajectories and velocities of the particles.

Particles Dynamic Behavior in the Turbine Stage

The dimensions of the stator and rotor of the turbine stage are given in Figure 12, while the airfoil dimensions are given in Reference 27. Figure 13 illustrates the combined gas velocity diagram for the 53.42% degree of reaction turbine stage. The mesh structure used for the calculation of the gas properties and the particle trajectories is shown in Figure 14. The particles are assumed to enter the turbine stator with uniform velocity. The particle concentration α does not appear in the equations of motion of the particles, hence it does not influence the behavior of any individual particle for practically small concentrations. Associated with certain α, and suspension flow rate are specific spacings between particles, which determine the place and the frequency of collisions and consequently affects the rate of blade erosion at the different points on its surface. Since the blade rotational speed is much higher than the particle velocity at the entrance to the turbine rotor, the position of the rotor blades may be taken arbitrarily (Figure 12). The dynamic behavior of a group of five particles of mean diameter d_p = 200 microns, entering the stator blade uniformly is shown in Figures 15, 16, 17 and 18. In particular, the projection of the absolute and relative trajectories in the stream surface of revolution and the radial displacement and the nondimensional absolute particle velocity distribution through the stage is illustrated in these figures. Similar figures for eleven particles uniformly entering the stator cascade with mean diameters 40 microns and 8 microns are given in Figures 19 to 22 and 23 to 26, respectively. In the case of the particles of d_p = 200 microns, the results are only plotted for every other particle in order to facilitate interpretation of the figures. In Figures 15 through 26, the particle material density ρ_p is 68.7 lb/ft^3 and the initial particle absolute velocity ratio, nondimensionalized with respect to gas inlet velocity, C_{p_i}/C_{g_i} equals 0.3. The gas conditions at the turbine stator inlet are: gas initial velocity C_{g_i} = 142.64 ft/sec, initial gas density $\rho_{g_{in}}$ = 0.076 lb/ft^3, initial gas total temperature $T_{g_{in}}$ = 60°F, and the total mass flow rate per channel W = 0.123 lb/sec.; and the particles enter at the stream surface of revolution of radius 7.05 inches The diameter of the turbine is taken relatively small so that the centrifugal effects on the particles are pronounced and in order to give a more general particle path. The cascade design angular speed at the mid-radius R is taken to be ω_d = 603.5 radians per second, which is equivalent to a mid-radius blade velocity of 352.5 ft/sec. From Figures 15 through 26 it can be observed that as the particle mean diameter decreases, the

particles experience less deviation from the gas streamlines in the stator. They tend to enter the opposite rotor blade channel and experience less scattering in the rotating nozzles (Figures 16, 20 and 24). Particles with higher mean diameters hit the blunt leading edge of the rotor blade and return to the stator, collide with the stator suction surface and return to the rotor. They may repeat the same process more than one time, causing erosion of the suction side of the stator blades (particles number 2, 4, 6 and 8 in Figure 15). The particles enter the rotor when they pick up enough speed to take them through the rotor nozzles. The band that contains the particles as they leave the stator narrows as the particle mean diameter decreases (compare Figures 15 and 23 for d_p = 200 and 8 microns, respectively). As the particles mean diameter decrease, they attain higher velocities in the stator and the change in their absolute velocities as they enter the rotor decrease (Figures 18, 22 and 26). Particles with smaller mean diameters have smoother absolute and relative paths and velocity distributions, as can be seen from Figures 15 through 26. The velocity distributions of particles with smaller d_p, however, are more affected by the gas conditions, particularly near the stagnation points (Figure 26 for particles with d_p = 8 microns). Particles tend to move with a higher radial velocity after hitting the rotor blades. The higher the value of d_p, the higher will be the radial velocities of the particles after collision (Figures 17 and 25). The particles travel toward the blade tip as they pass through the stage. Those particles of d_p = 200 microns hit the turbine casing before leaving the turbine stage (Figure 17). Particles with d_p = 8 microns, however, travel through the stage without hitting the casing (Figure 25). The vertical lines in the relative trajectories of Figure 16 indicate the distances traveled by the rotor blades during the time taken by the particles to re-enter the stator, hit the stator blade suction side and reach the stator exit. These distances differ with the particle initial position and velocity as it returns to the stator. The loops in the curves of the particles velocity in Figure 18 are associated with the particles that return to the stator. These loops result from the particles momentum gain due to their collision with the rotor blades, followed by a momentum loss resulting from their impacts with the stator. Particles with d_p greater than 200 microns, tend to move back and forth many times from rotor to the stator and vice versa, until they either break into smaller particles, or reach the proper speed and direction to go through the rotor. It is also observed from Figures 15 and 16 for particles with d_p = 200 microns and Figures 23 and 24 for particles with d_p = 8 microns that, particles with smaller mean diameters experience fewer collisions with the stator and the rotor, particularly on the suction sides of the blades. Particle collisions with the blades due to their lateral motion are affected by the cascade geometry, namely, the pitch and blade camber. Other factors that influence these collisions are the mechanisms of impact and rebound, the cascade rotational speed, and gas and particle properties. The parts of the stator blade subjected to more impacts, and hence, higher rates of erosion, are the leading edge and pressure side. The stator blade suction side is subjected to impacts only from particles of higher mean diameters that return to the stator after hitting the rotor blade leading edge (Figure 15). In the rotor blades, the particles hit the blades with higher relative velocities, hence, the rate of erosion is expected to be higher than that for the stator blades. The rotor blade leading edge is eroded by particles of all sizes, while the pressure side is subjected to

collisions only from particles with higher mean diameters (Figures 16, 20 and 24). As the particles reach the casing, they impact and rebound in an occilating manner with decreasing amplitude. Finally, they move into the stream surface of revolution that passes through the blades tips and cause severe damage to blade tips in the later stages. The previous conclusions concerning the blade areas subjected to erosion are in agreement with the observations of actual eroded turbine blades.

In order to study the effects of different particulate flow parameters on the dynamic behavior of the particles, the particles are divided into three typical trajectory groups according to their location at the time they enter the stator. Figures 15, 19 and 23 or Figures 27, 32 and 37 illustrate typical examples of the three trajectory groups. In particular, particles such as number 2 start by hitting the upper part of the stator blade leading edge, particle number 6 moves straight in the stator channel and hits its pressure side, while particle number 10 starts by hitting the lower part of the turbine stator leading edge.

The dynamic behavior of particles having mean diameters of 200, 40 and 8 microns, the same material density and initial velocities, is investigated. The results are shown in Figures 27 to 41. The effect of particle mean diameter on it dynamic behavior is discussed above. Additional figures, showing the combined velocity diagrams of the particles as compared to those of the gas, are given for all of the typical particles (Figures 21, 36 and 31). These figures illustrate the difference in the overall behavior between the gas and the particles. In Figures 31, 36 and 41, V'_{p_1} and V'_{p_2} are the particle relative velocity components in the x-θ surface at the inlet and the exit from the rotor, respectively, while C'_{p_1} and C'_{p_2} represent their corresponding absolute values. The particle radial velocity components are written next to the corresponding velocity diagrams.

The effect of particle material density, $\bar{\rho}_p$, on the dynamic behavior of the solid particles is shown in Figures 42 through 53. The dynamic behavior of the three typical particles is shown in three groups of four figures each for $\bar{\rho}_p$ = 34, 68.7 and 151 lb/ft^3 for a constant d_p = 40 microns and C_{p_i}/C_{g_i} = 0.3. These particle material densities approximately correspond to the densities of coal, sand, and silicon, which are the materials that a practical gas turbine flow may contain as solid suspension. It may be shown from the above figures that a decrease in $\bar{\rho}_p$ will lessen the deviation between the particle trajectory and the gas streamlines (Figures 42, 46 and 50), decrease their radial displacements (Figures 44, 48 and 52), and increase their initial acceleration (Figures 45, 49 and 53). Since particles with smaller $\bar{\rho}_p$ tend to escape collision with the rotor blades, they experience fewer abrupt changes in their velocity as they pass through the rotor (Figure 53).

For particles with constant d_p = 40 microns and $\bar{\rho}_p$ = 68.7 lb/ft^3, the initial nondimensional absolute particle velocity C_{p_i}/C_{g_i} is varied, taking the values 0.15, 0.3 and 0.6 to determine the effect of C_{p_i}/C_{g_i} on

the particle dynamic behavior. The dynamic behaviors of the three typical particles are plotted in Figures 54 through 65. These figures show that the particle initial speed have a small effect on their trajectories, especially in the stator. The particles are found to reach the same absolute velocity after traveling relatively short distances irrespective of their initially different value of C_{p_i}/C_{g_i} (Figure 57). The effect of the initial gas velocity on the dynamic behavior of solid particles may be determined from the figures for different C_{p_i}/C_{g_i}, bearing in mind that for the same inlet particle velocity, higher gas inlet velocity would mean lower C_{p_i}/C_{g_i}, and vice versa.

The particle mean diameter is the parameter that has the greatest effect on the particles dynamic behavior, while ρ_p and C_{p_i}/C_{g_i} have smaller effects. The same conclusion could be arrived at by looking at the equations of motion of the particles, since d_p appears raised to the second power.

CONCLUSION

The dynamic behavior of solid particles entrained by the compressible gas flow in a stationary or rotating cascade of a turbine is determined. Impacts of the solid particles with the blades and the casing are considered. The equations of motion of the solid particles are solved in the three dimensional space. The drag forces on the particles are calculated using drag formulas that fit the drag curve of a spherical particle over a wide range of the Reynolds numbers. The compressible gas flow properties are computed by solving numerically the gas equations of motion in a blade to blade surface of revolution of a rotating cascade. Experimental investigation is made to study the impact and rebound phenomenon of the particles from the walls, to determine formulas for the restitution ratio, and rebound to incidence angle ratio. These formulas define the particle conditions after collision which are then used to continue the solution of the equations of motion for the particles. These formulas have to be determined experimentally for every particle-target material combination once the turbomachine operating condition is known.

The study showed that in general, solid particle paths are deviated from gas streamlines. This deviation increases with increased particle mean diameter, material density, particle initial velocity or decreased gas initial velocity. The particle mean diameter has the greatest effect on the dynamic behavior of the particles, while the particle material density has a lesser effect and the particle initial velocity has the least effect.

The turbine stator and rotor blade leading edges and pressure sides will be eroded by particles of all sizes. The rear part of the stator suction side will be eroded by larger particles after their return to the stator due to their collision with the rotor blades. The turbine rotor is expected to suffer more severe erosion than the stator due to the higher velocities of the particles in the rotor.

Turbines may be designed to both minimize erosion as well as optimizing aerodynamic characteristics using the results of this investigation. Means may be introduced to collect or deviate some of the particles, expecially those that contribute most to erosion, from the blades and hence, reduce erosion damage.

REFERENCES

1. Lapple, C.E. and Shepherd, C.B., "Calculation of Particle Trajectories," Industrial and Engineering Chemistry, Vol. 32, No. 5, May 1940, pp. 605-617.

2. Gilbert, M., Davis, L. and Altman, D., "Velocity Lag of Particles in Linearly Accelerated Combustion Gases," Jet Propulsion, Vol. 25, January 1955, pp. 25-30.

3. Kriebel, A.R., "Particle Trajectories in a Gas Centrifuge," Transactions of the ASME, Journal of Basic Engineering, Series D, September 1961, pp. 333-340.

4. Neilson, J.H. and Gilchrist, A., "An Analytical and Experimental Investigation of the trajectories of Particles Entrained by the Gas Flow in Nozzles," Vol. 35, Part 3, 1969, pp. 549-559.

5. Vitols, V., "Determination of Theoretical Collection Efficiencies of Aspirated Particulate Matter Sampling Propes Anisokinetic Flow," Ph.D. Thesis, the University of Michigan, 1964.

6. Tabakoff, W. and Hussein, M.F., "Trajectories of Particles Suspended in Fluid Flow Through Cascades," AIAA Journal of Aircraft, Vol. 8, No. 1, January 1971.

7. Tabakoff, W., Hamed, A. and Hussein, M.F., "Investigation of Gas Particle Flow Pressure and Solid Particle Trajectories and Velocities in an Axial Flow Cascade Pair," ASME Paper No. 72-GT-57, presented at the ASME 17th Annual International Gas Turbine Conference and Product Show, San Francisco, California, March 1972.

8. Hussein, M.F., and Tabakoff, W., "Calculation of Particle Trajectories in a Stationary Two Dimensional Cascade," Project Themis Report No. 72-27, University of Cincinnati, Cincinnati, Ohio, 1972, USGRD Report to be published.

9. Hussein, M.F. and Tabakoff, W., "Computer Program to Estimate the Dynamic Characteristics of Solid Particles Entrained by the Gas Flow in a Rotating Cascade of a Turbomachine," United States Government Research and Development Report to be published.

10. Soo, S.L., "Fluid Dynamics of Multiphase Systems," Blaisdell Publishing Company, 1967.

11. Tchen, C.M., "Mean Value and Correlation Problems Connected with the Motion of Small Particles Suspended in a Turbulent Fluid, Dissertation, Martinus Nijhoff, The Hague, 1947.

12. Hinze, J.O., "Turbulence" McGraw-Hill, New York, 1959.

13. Corrsin, S. and Lumley J., "On the Equations of Motion for a Particle in Turbulent Fluid," Applied Scientific Research 6A, 114, (1956).

14. Lumley, J.L., "Some Problems Connected with the Motion of Small Particles in Turbulent Fluid," Ph.D. Thesis, Johns Hopkins University, 1957.

15. Hussein, M.F. "The Dynamic Characteristics of Solid Particles in Particulate Flow in Rotating Turbomachinery," Ph.D. Dissertation, University of Cincinnati, Cincinnati, Ohio, 1972.

16. Schlichting, H., "Boundary Layer Theory," McGraw-Hill, Inc., 1968.

17. Davis, D.S., "Nomography and Emperical Equations," Reinhold Publishing Corp., 1962.

18. Kane, T.R., "Dynamics," Holt, Rinehart and Winston, Inc., 1968.

19. Marris, A.W. and Stonking, C.E., "Advanced Dynamics," McGraw-Hill Inc., 1967.

20. Vavra, M.H., "Aerothemodynamics and Flow in Turbomachines," John Wiley and Sons, Inc., 1960.

21. Varga, R.S., "Matrix Iterative Analysis," Prentice-Hall, Inc., 1962.

22. Katsanis, T., "Computer Program for Calculation Velocities and Streamlines on a Blade to Blade Stream Surface of a Turbomachine," NASA - TN D - 4525, April 1968.

23. Bueckner, H.F. and Schnackel, H.C., "The Calculation of Incompressible Flow through Turbine Cascades," ASME Paper presented at the ASME, 1959 Annual Meeting, Atlantic City, New Jersey, Nov. 1959.

24. Schlichting, H., "Berechnung der reibungslosen inkompressiblen Strömung für ein vorgegebenes ebenes Schaufelgitter," VDI-Forschungsheft 447 (1955).

25. Shapiro, A.H., "The Dynamics and Thermodynamics of Compressible Fluid Flow," The Ronald Press Company, 1953.

26. Imbach, H.E., "Calculation of Compressible, Frictionless Subsonic Flow Through a Plane Blade Cascade," The Brown Boveri Review, Vol. 51, No. 12, December 1964.

27. Tabakoff, W., and Hussein, M.F., "An Experimental Study of the Effect of Solid Particles on the Pressure at the Blade Surface in Cascade," USGRD Report No. AD-703896, STAR Report No. N70-31319.

$$C_D = \frac{24}{Re} \qquad 0 < Re \leq 1.0$$

$$C_D = \frac{24}{Re}\left(1 + \frac{3}{16} Re\right) \qquad 1.0 < Re \leq 4.0$$

$$C_D = (21.9416\, Re^{-0.718} + 0.3246) \qquad 4.0 < Re \leq 2000$$

$$C_D = 0.4 \qquad Re > 2000$$

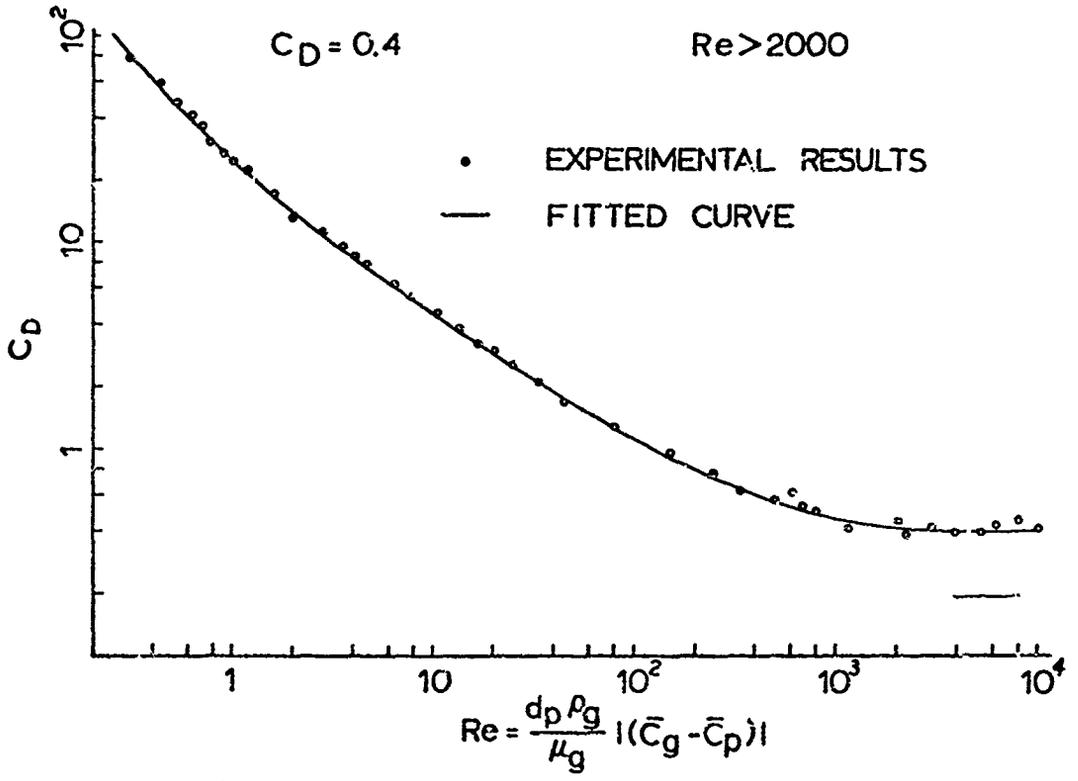

FIG. 1 DRAG COEFFICIENT FOR SPHERICAL PARTICLE

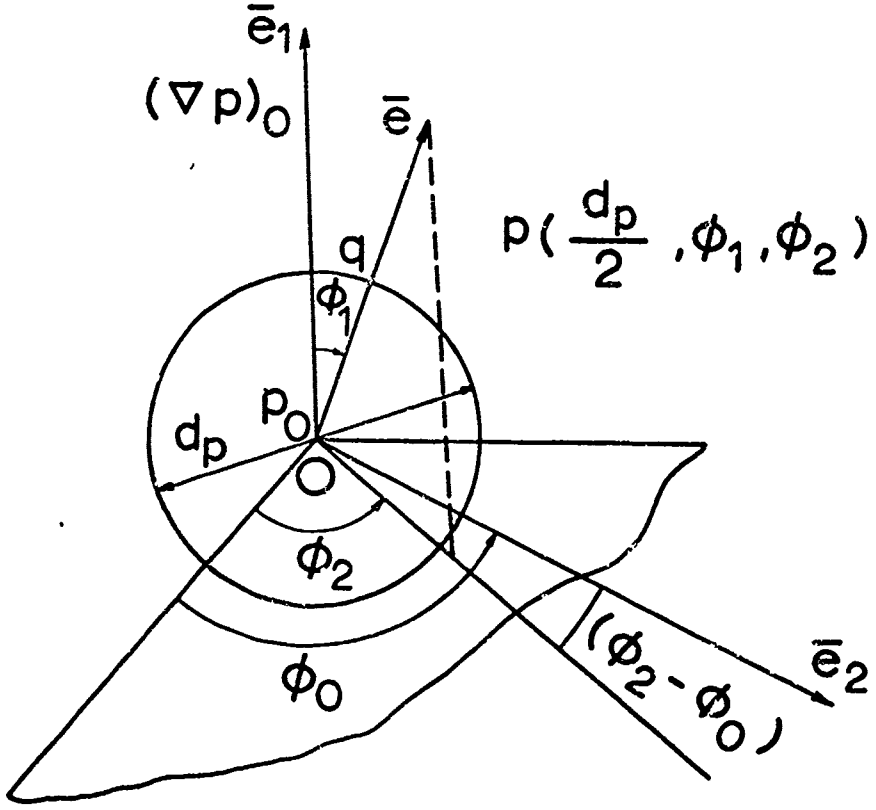
$\bar{e}_1$
$(\nabla p)_0$
$\bar{e}$
$p(\frac{d_p}{2}, \phi_1, \phi_2)$
q
ϕ_1
d_p
p_0
O
ϕ_2
ϕ_0
$(\phi_2 - \phi_0)$
$\bar{e}_2$

FIGURE 2

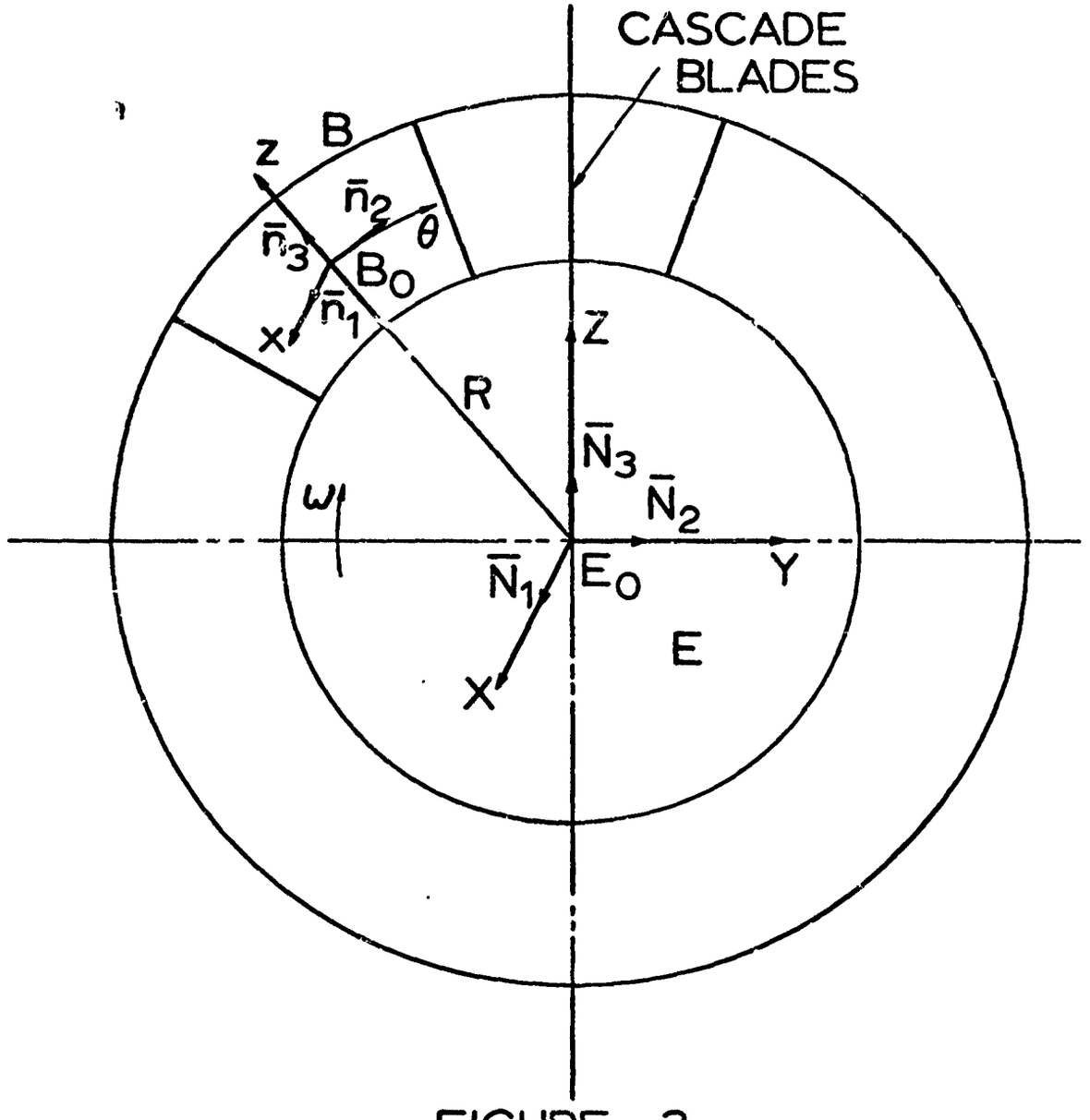

FIGURE 3

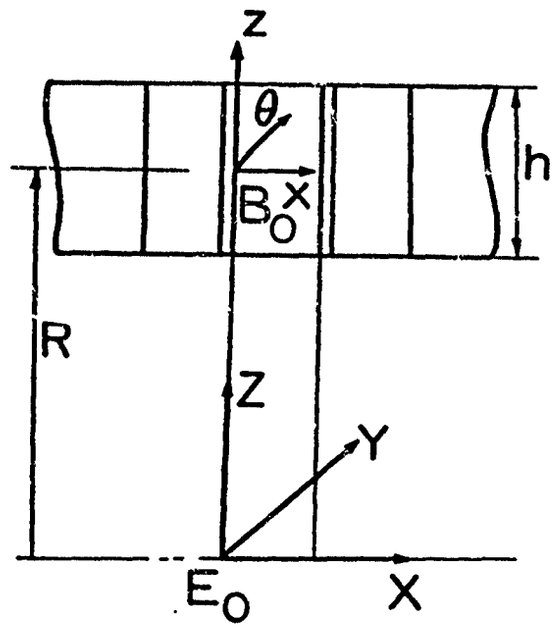

FIGURE 4

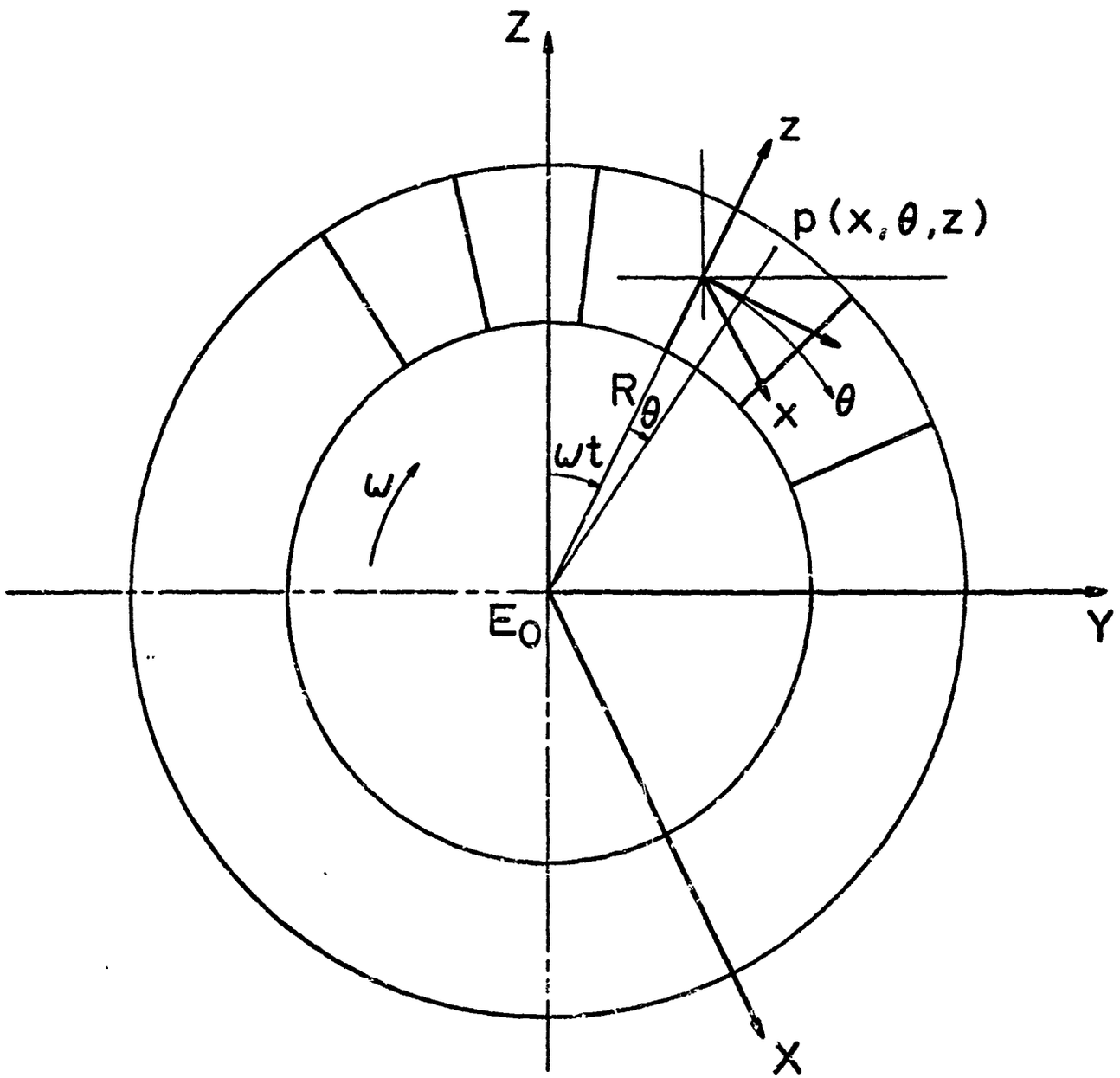

FIGURE 5

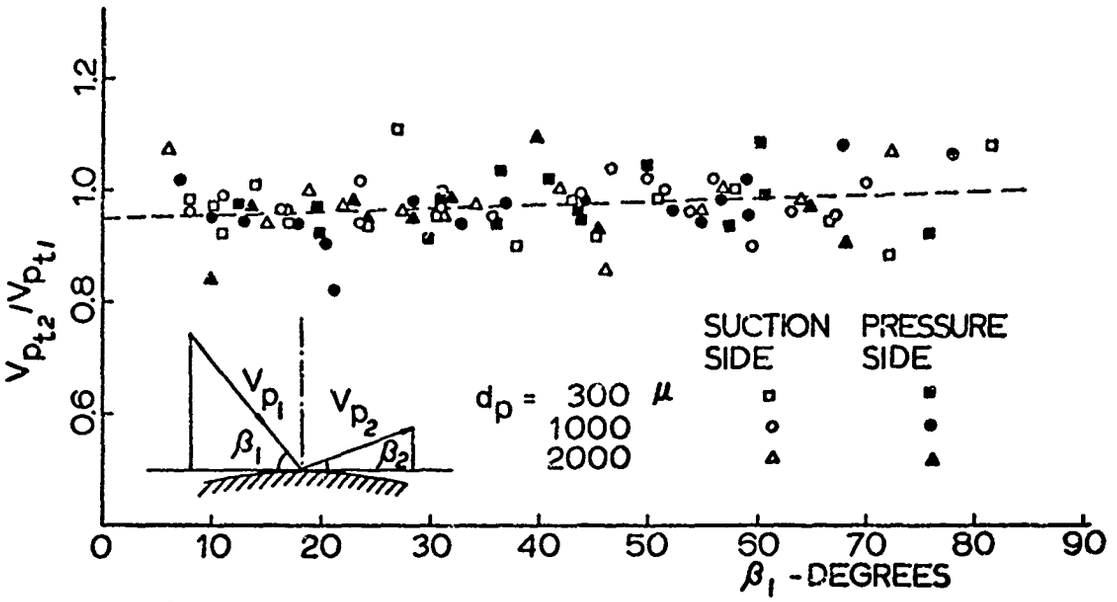

FIG. 6 DROP IN PARTICLE RELATIVE TANGENTIAL VELOCITY DUE TO COLLISION

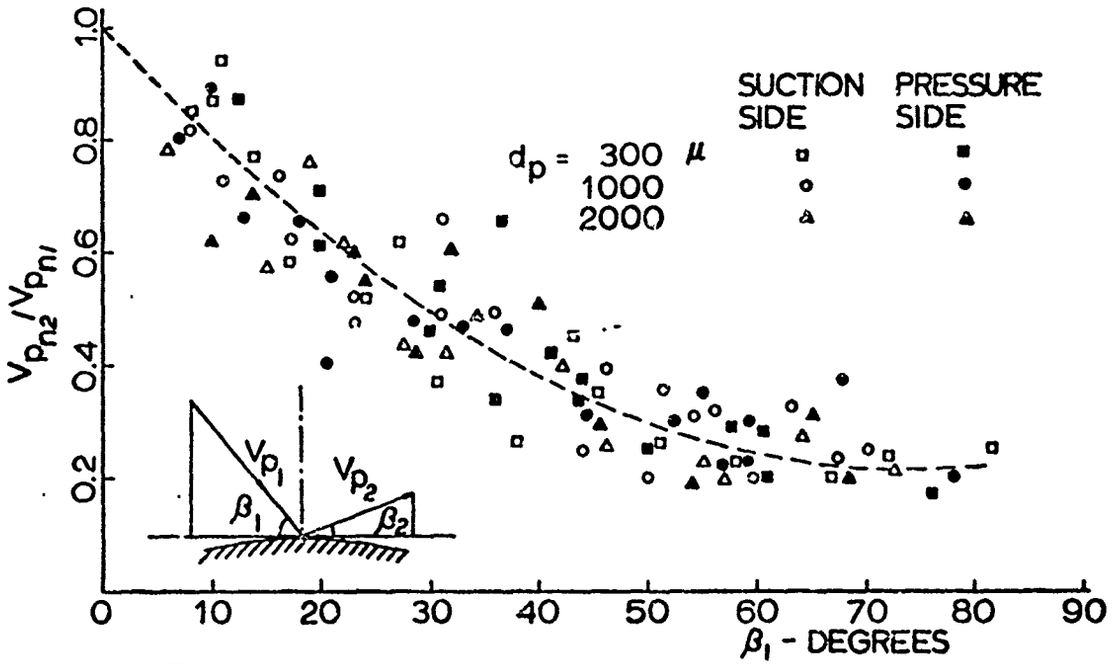

FIG. 7 DROP IN PARTICLE RELATIVE NORMAL VELOCITY DUE TO COLLISION

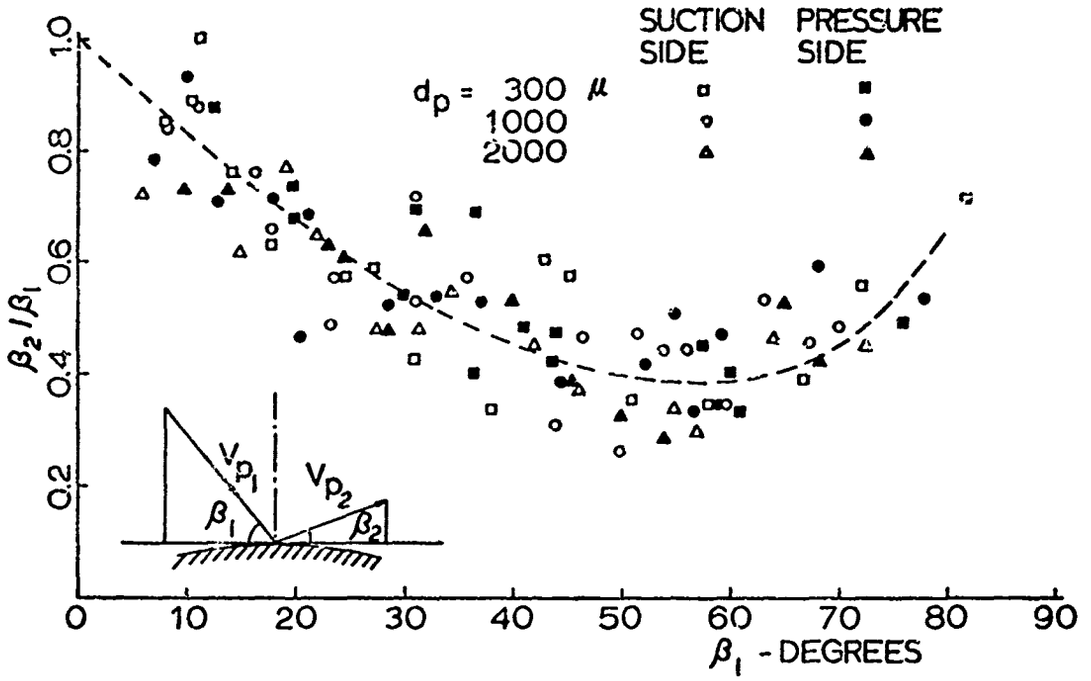

FIG. 8 NONDIMENSIONAL ANGLE OF REBOUND

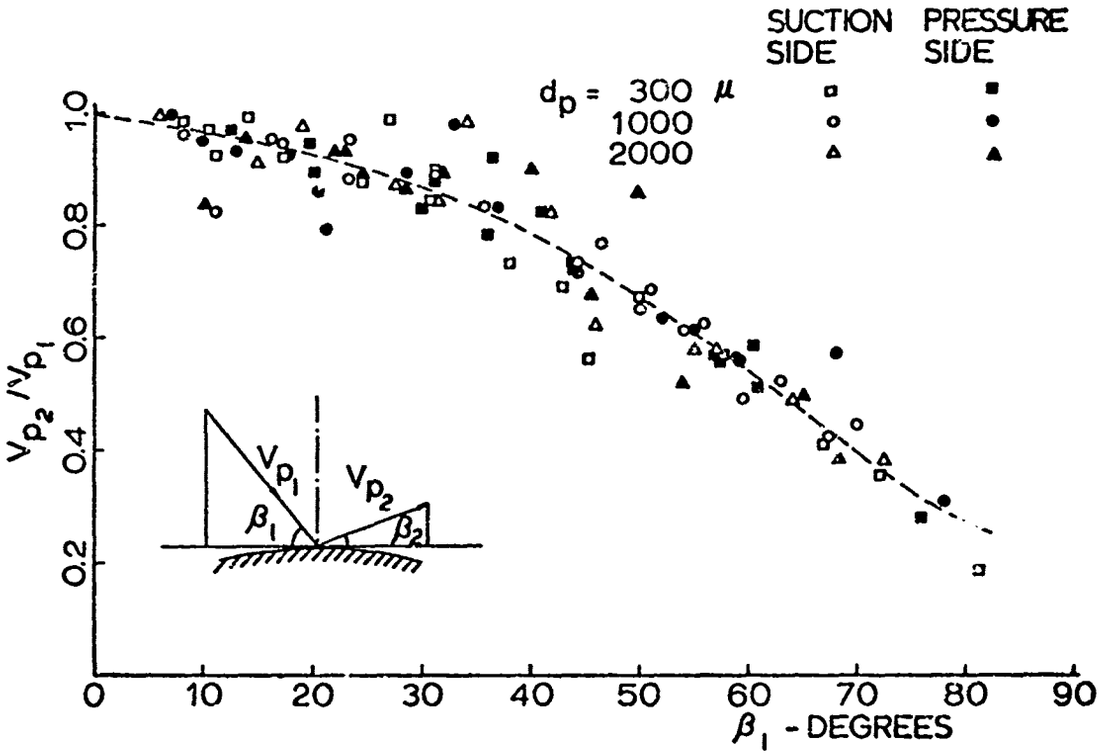

FIG. 9 DROP IN PARTICLE RELATIVE VELOCITY DUE TO COLLISION (RESTITUTION RATIO)

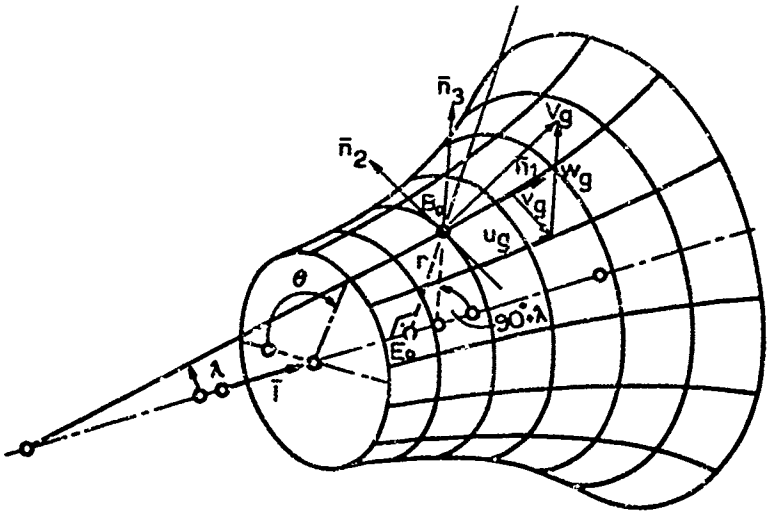

FIGURE 10 AXSYMMETRIC COORDINATE SURFACE

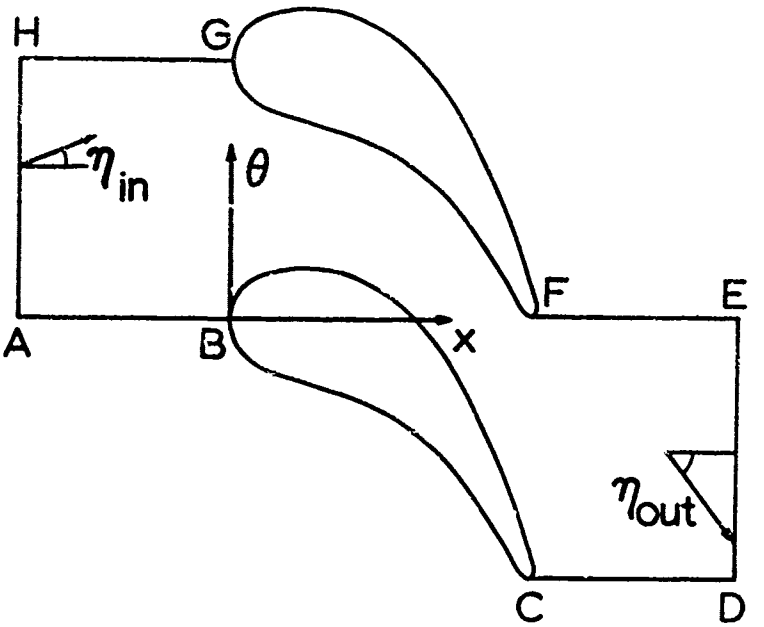

FIGURE 11 GAS FLOW CONTROL VOLUME

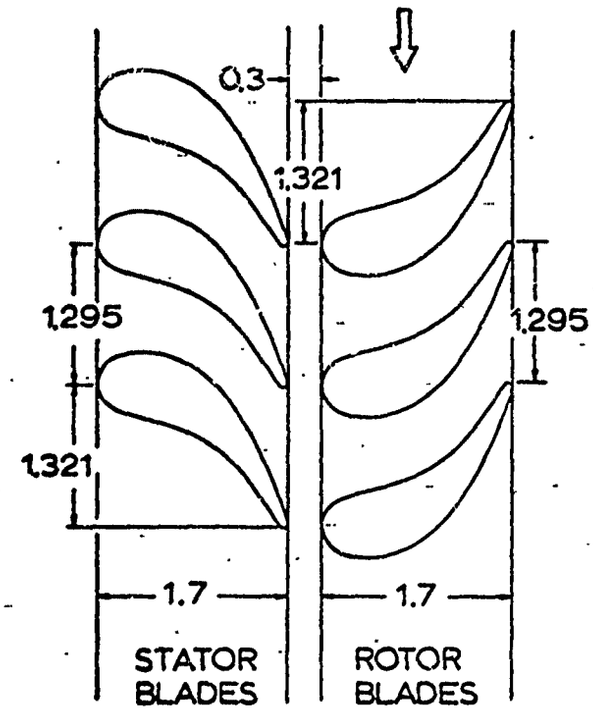

FIGURE 12 TURBINE STAGE DIMENSIONS

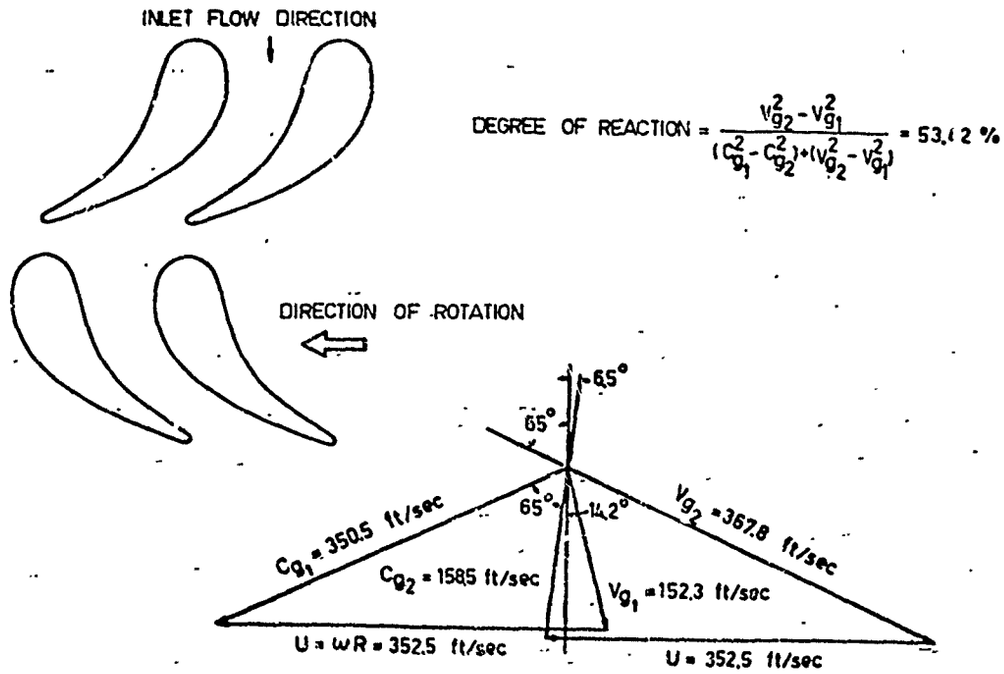

FIGURE 13 COMBINED GAS VELOCITY DIAGRAM (TURBINE STAGE)

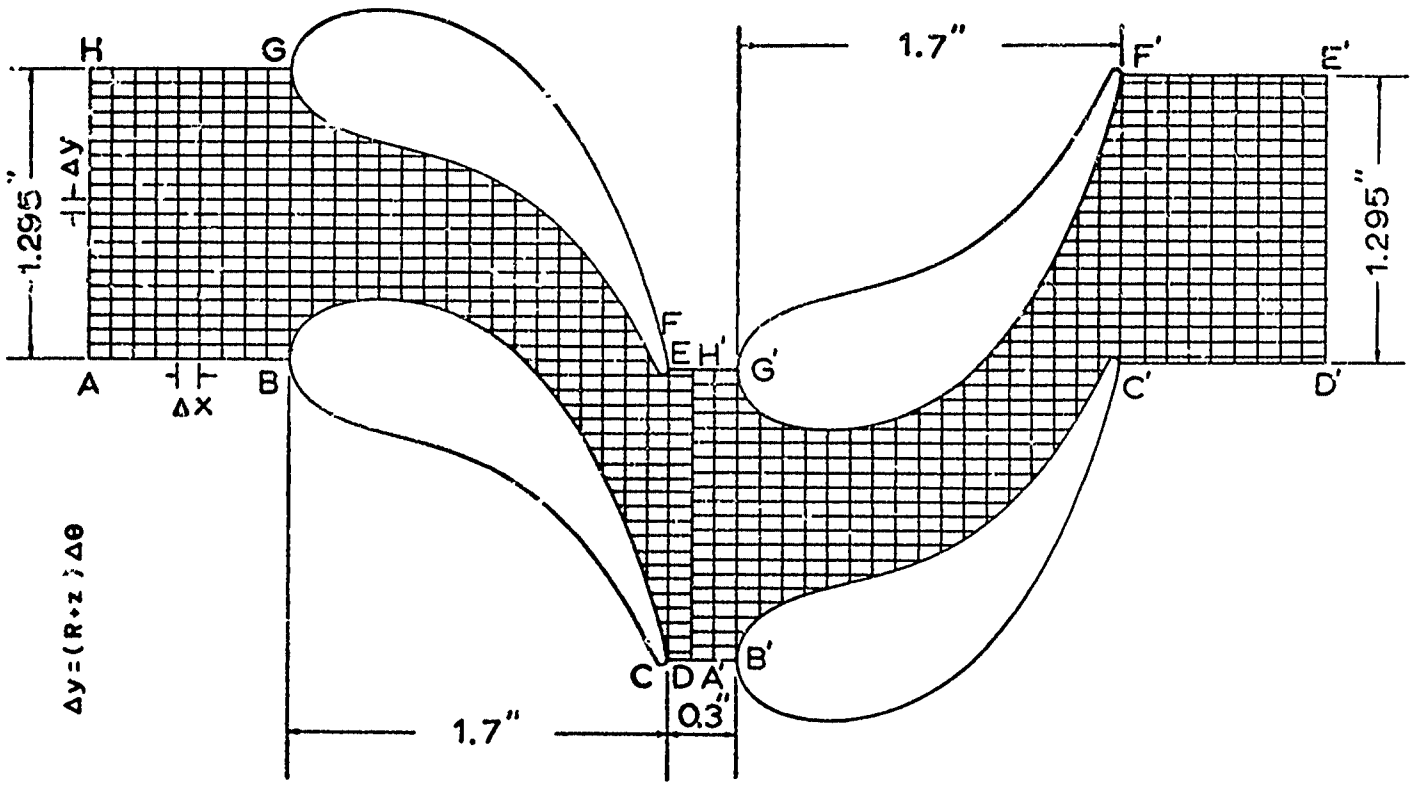

FIGURE 14 MESH POINTS FOR TURBINE BLADING

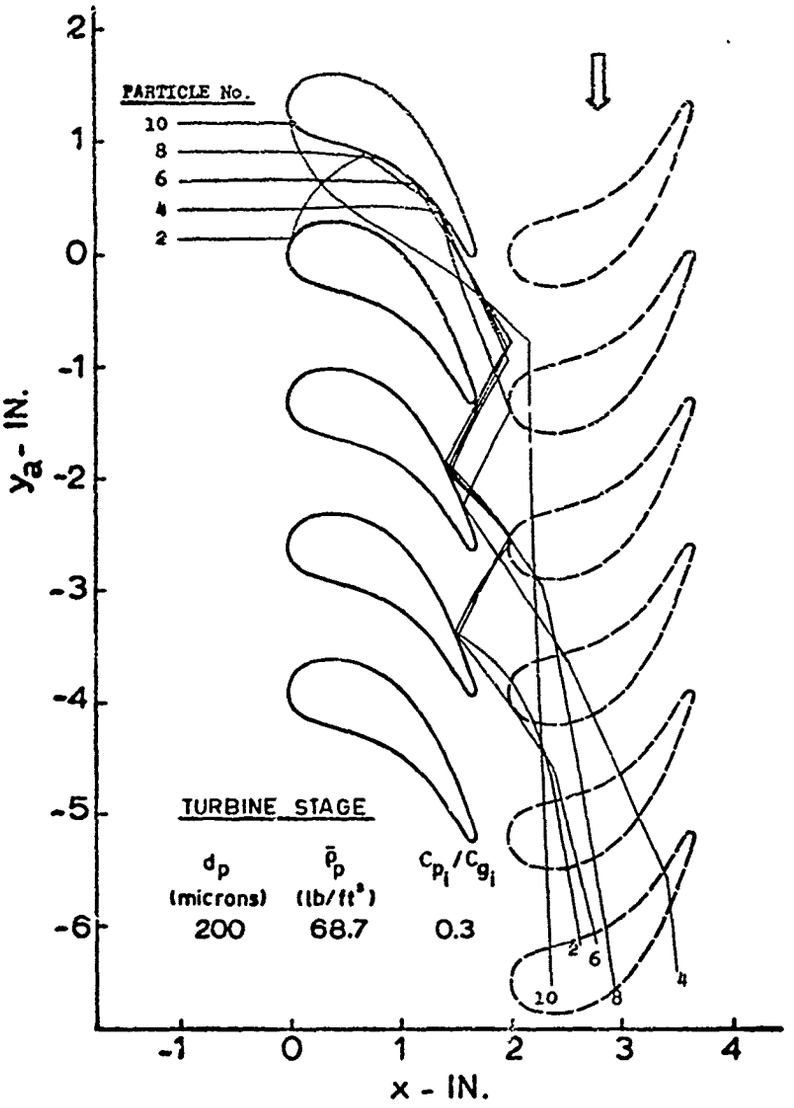

FIGURE 15 AXIAL AND TANGENTIAL COMPONENTS OF PARTICLE TRAJECTORIES

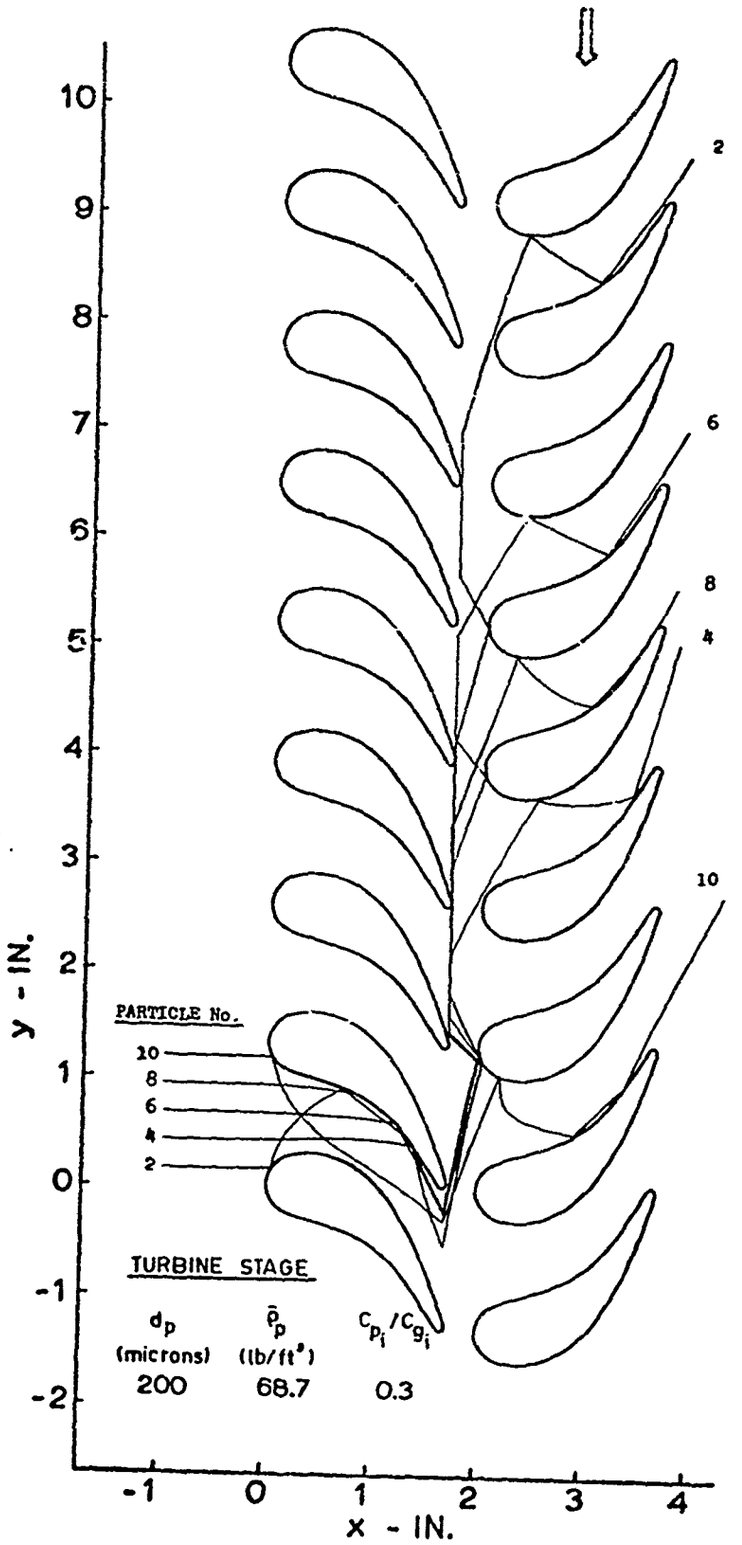

FIGURE 16 AXIAL AND TANGENTIAL COMPONENTS OF PARTICLE TRAJECTORIES RELATIVE TO THE ROTOR BLADES

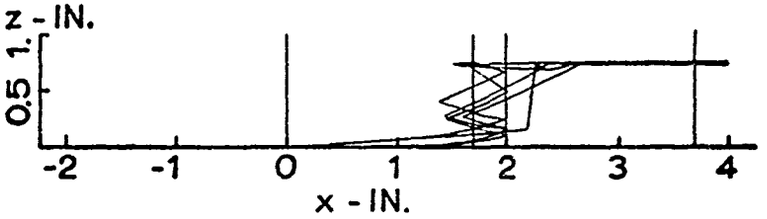

FIGURE 17 AXIAL AND RADIAL COMPONENTS OF PARTICLE TRAJECTORIES

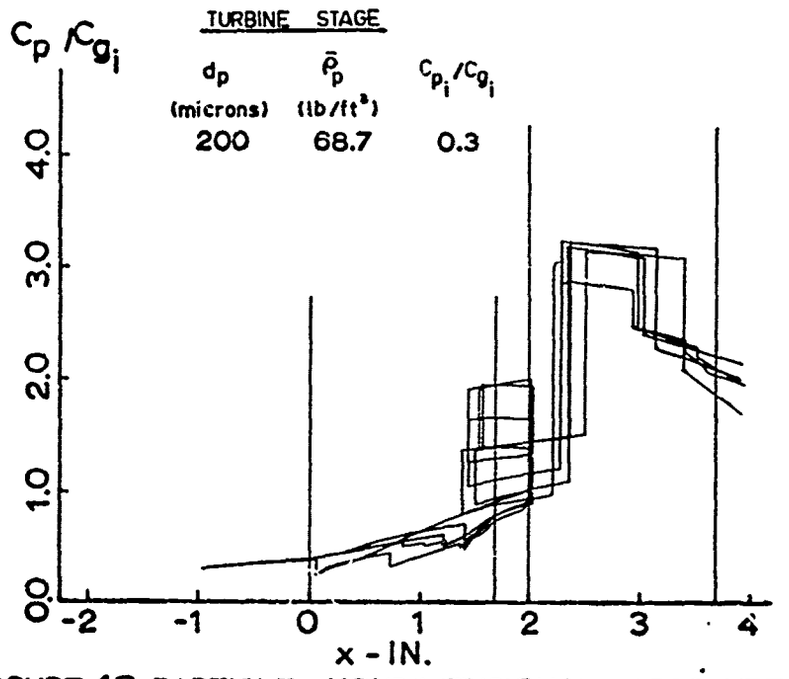

FIGURE 18 PARTICLE NONDIMENSIONAL ABSOLUTE VELOCITIES

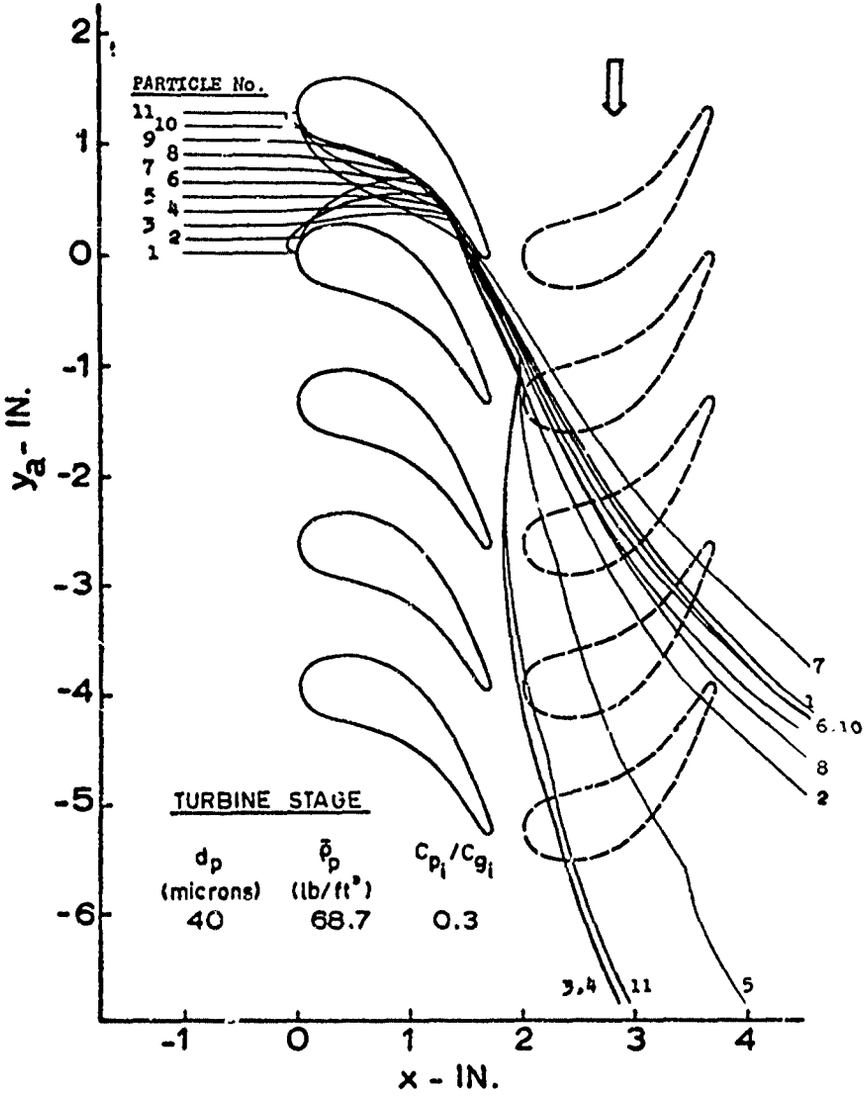

FIGURE 19 AXIAL AND TANGENTIAL COMPONENTS OF PARTICLE TRAJECTORIES

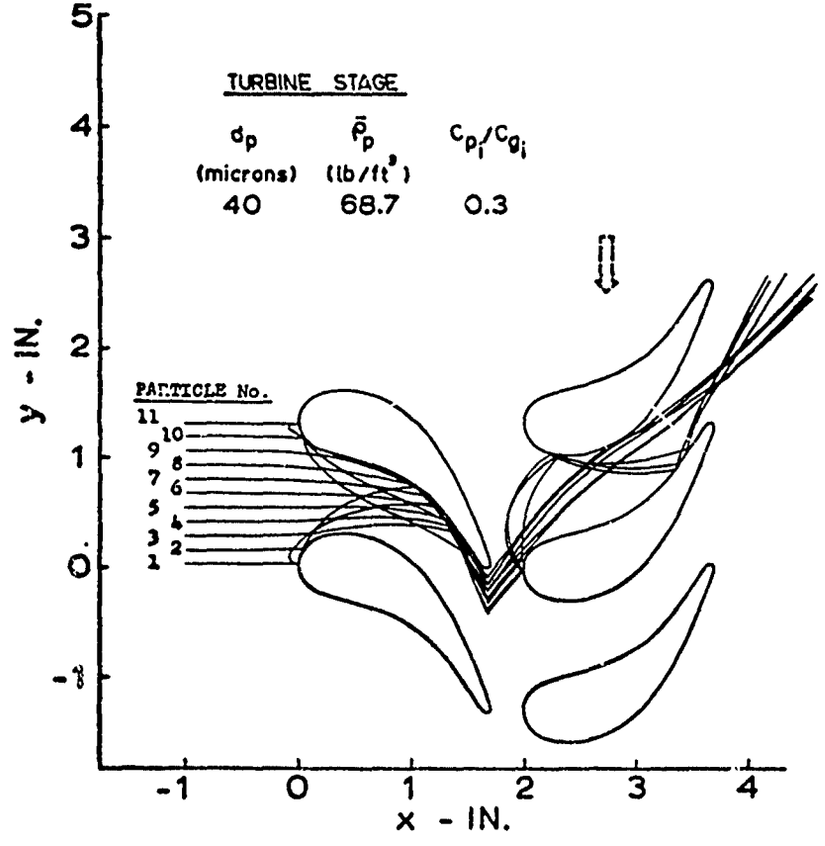

FIGURE 20 AXIAL AND TANGENTIAL COMPONENTS OF PARTICLE TRAJECTORIES RELATIVE TO THE ROTOR BLADES

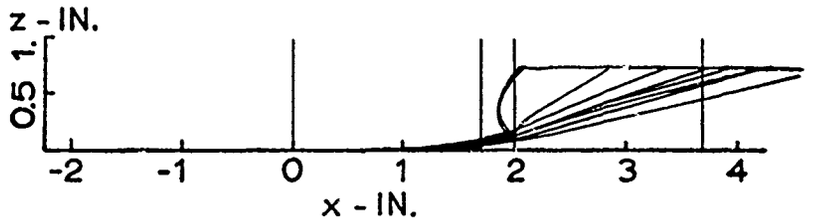

FIGURE 21 AXIAL AND RADIAL COMPONENTS OF PARTICLE TRAJECTORIES

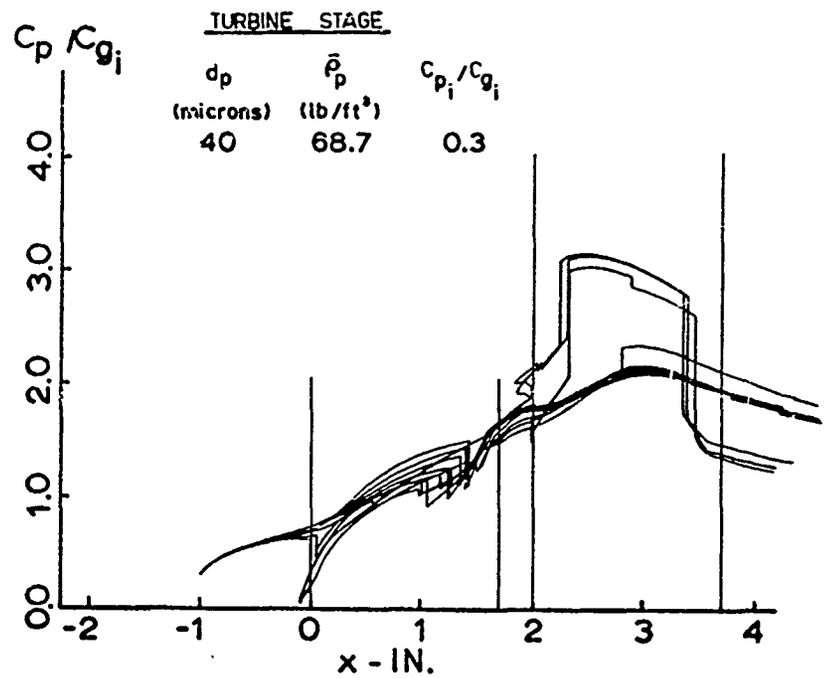

FIGURE 22 PARTICLE NONDIMENSIONAL ABSOLUTE VELOCITIES

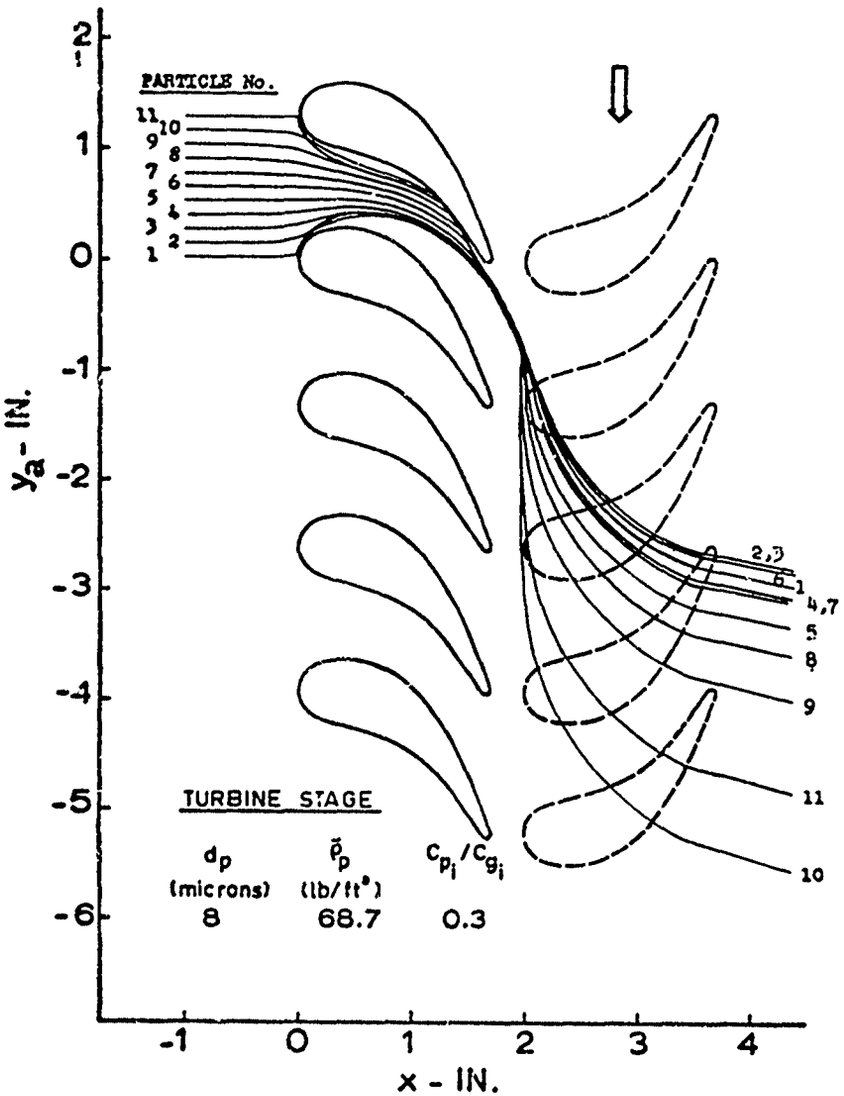

FIGURE 23 AXIAL AND TANGENTIAL COMPONENTS OF PARTICLE TRAJECTORIES

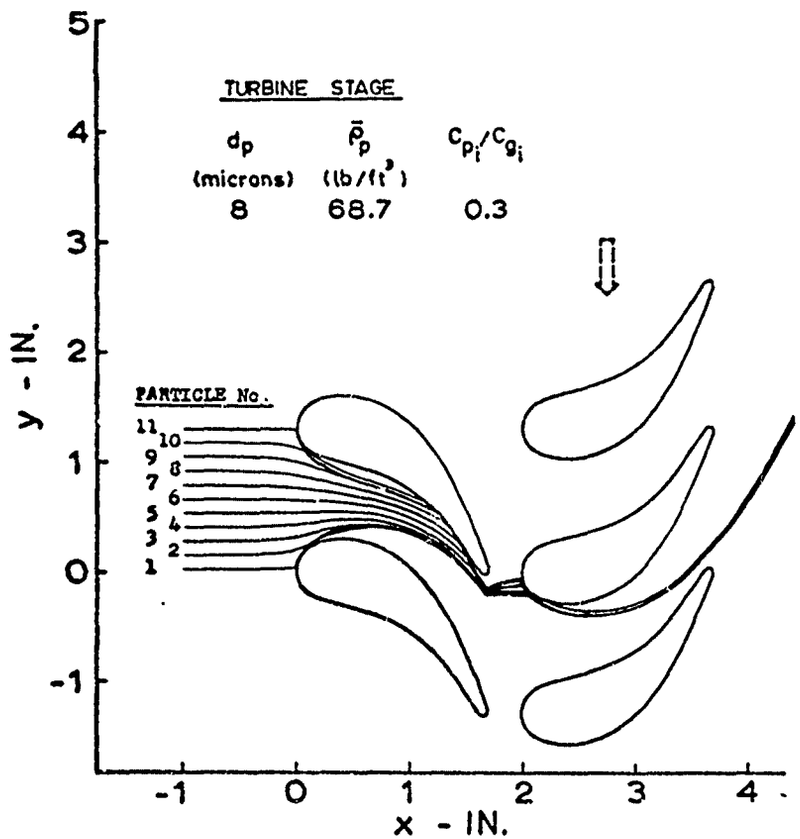

FIGURE 24 AXIAL AND TANGENTIAL COMPONENTS OF PARTICLE TRAJECTORIES RELATIVE TO THE ROTOR BLADES

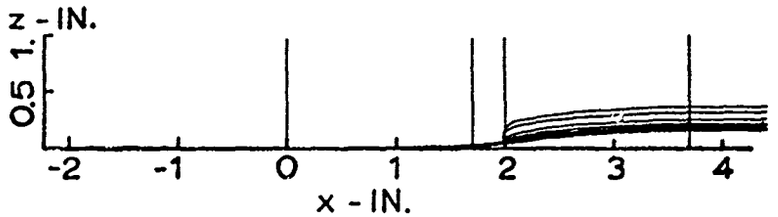

FIGURE 25 AXIAL AND RADIAL COMPONENTS OF PARTICLE TRAJECTORIES

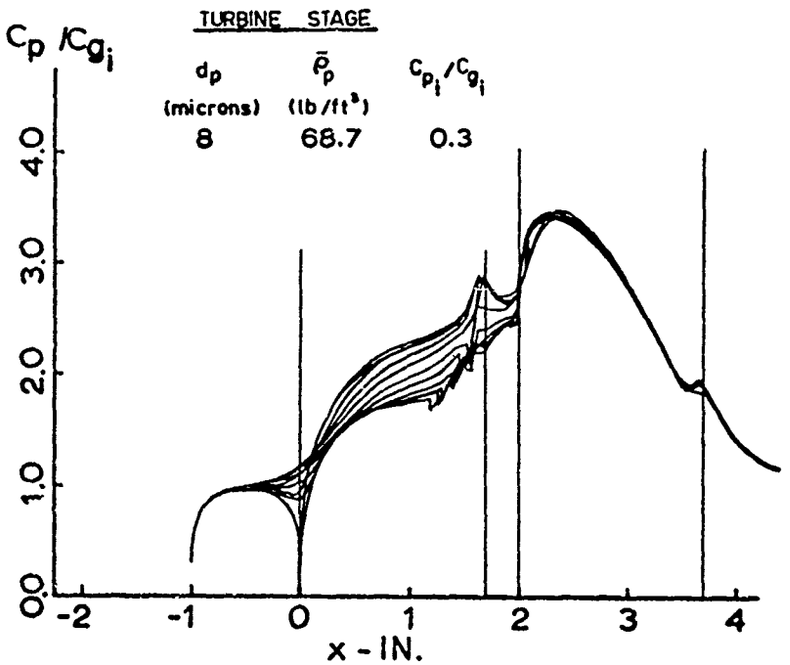

FIGURE 26 PARTICLE NONDIMENSIONAL ABSOLUTE VELOCITIES

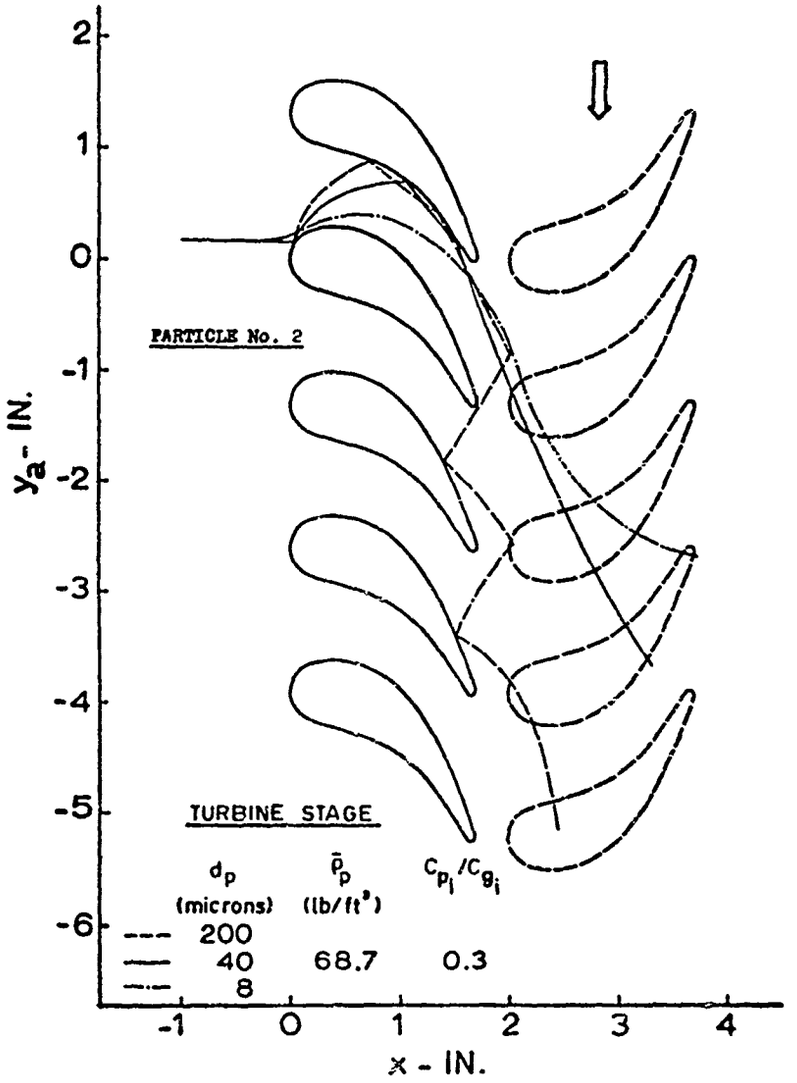

FIGURE 27 AXIAL AND TANGENTIAL COMPONENTS OF PARTICLE TRAJECTORIES (EFFECT OF d_p)

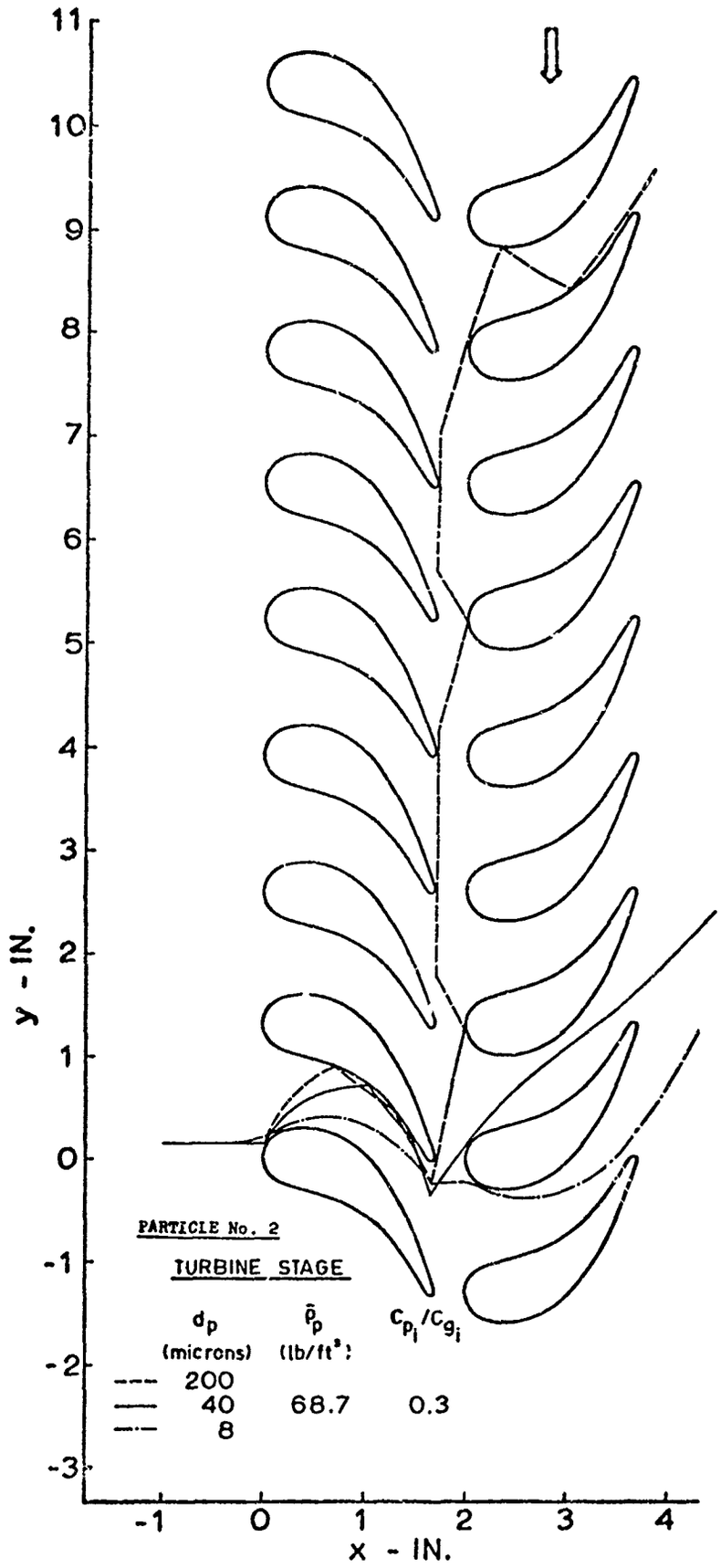

FIGURE 28 AXIAL AND TANGENTIAL COMPONENTS OF PARTICLE TRAJECTORIES RELATIVE TO THE ROTOR BLADES (EFFECT OF dp)

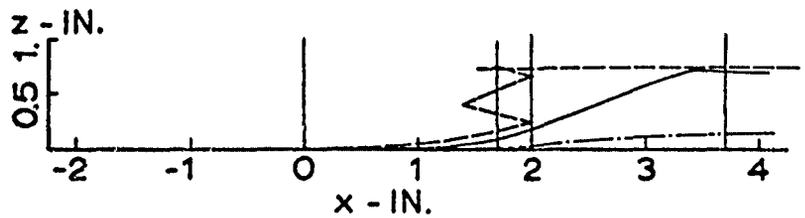

FIGURE 29 AXIAL AND RADIAL COMPONENTS OF PARTICLE TRAJECTORIES

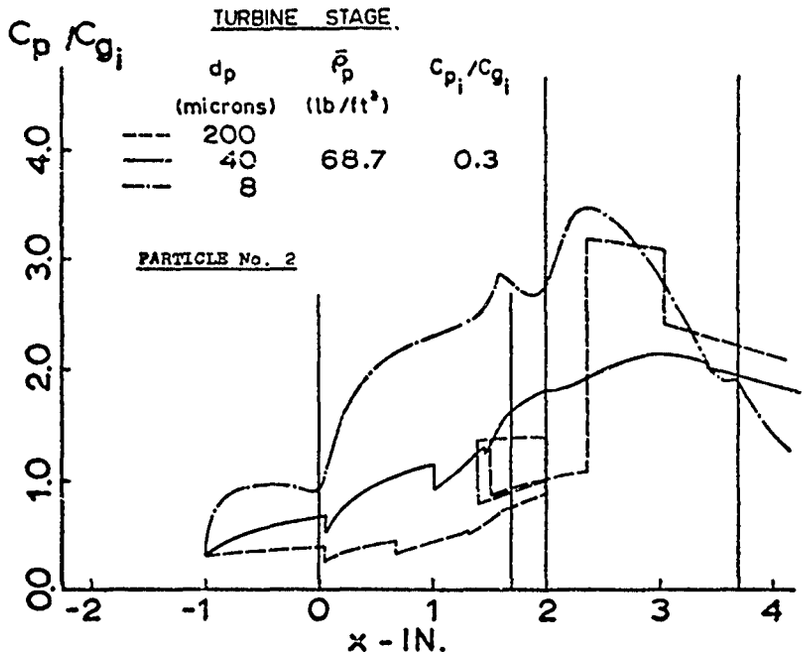

FIGURE 30 PARTICLE NONDIMENSIONAL ABSOLUTE VELOCITIES (EFFECT OF d_p)

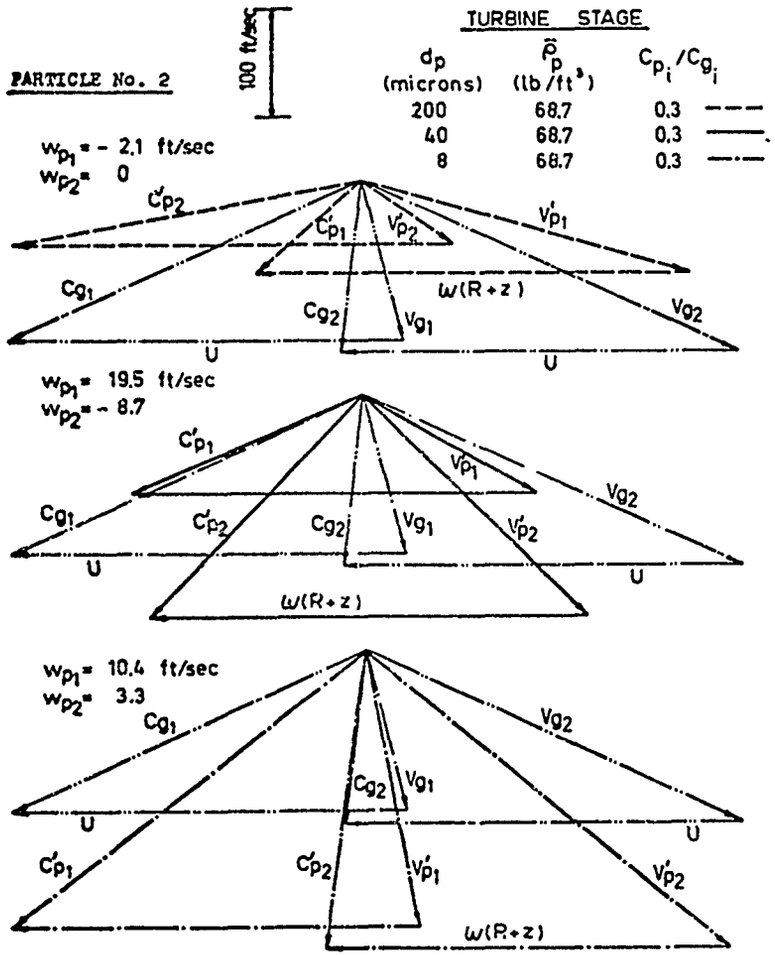

FIGURE 31 PARTICLE VELOCITY DIAGRAM

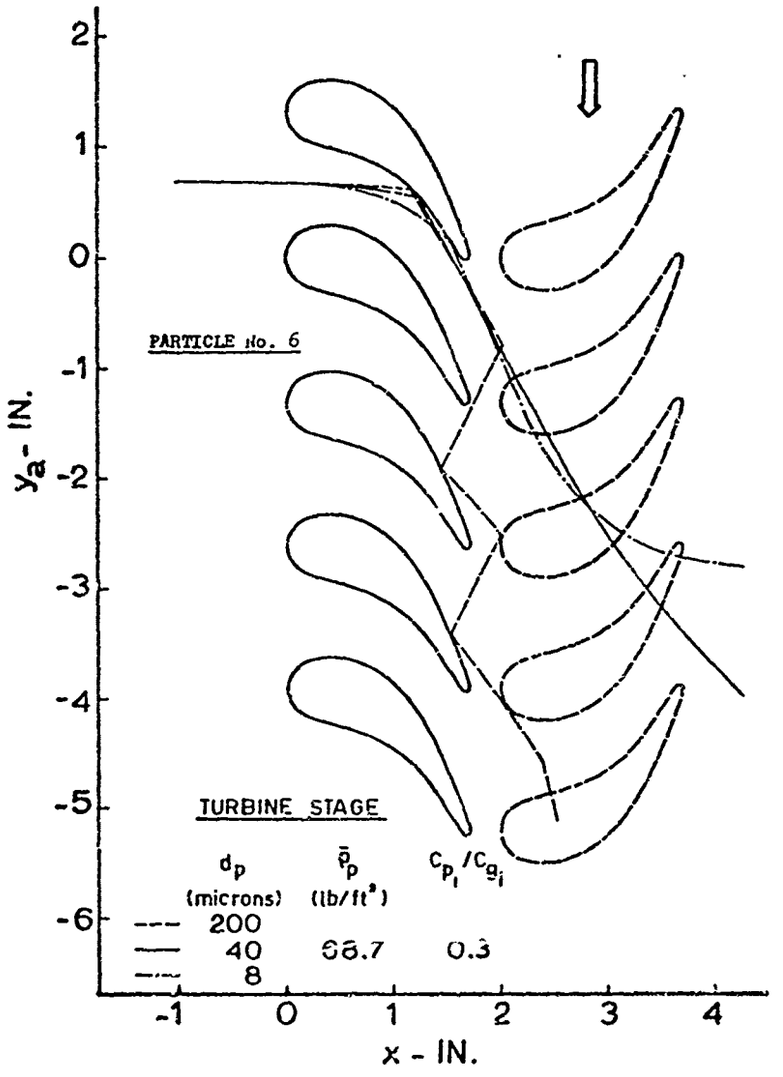

FIGURE 32 AXIAL AND TANGENTIAL COMPONENTS OF PARTICLE TRAJECTORIES (EFFECT OF d_p)

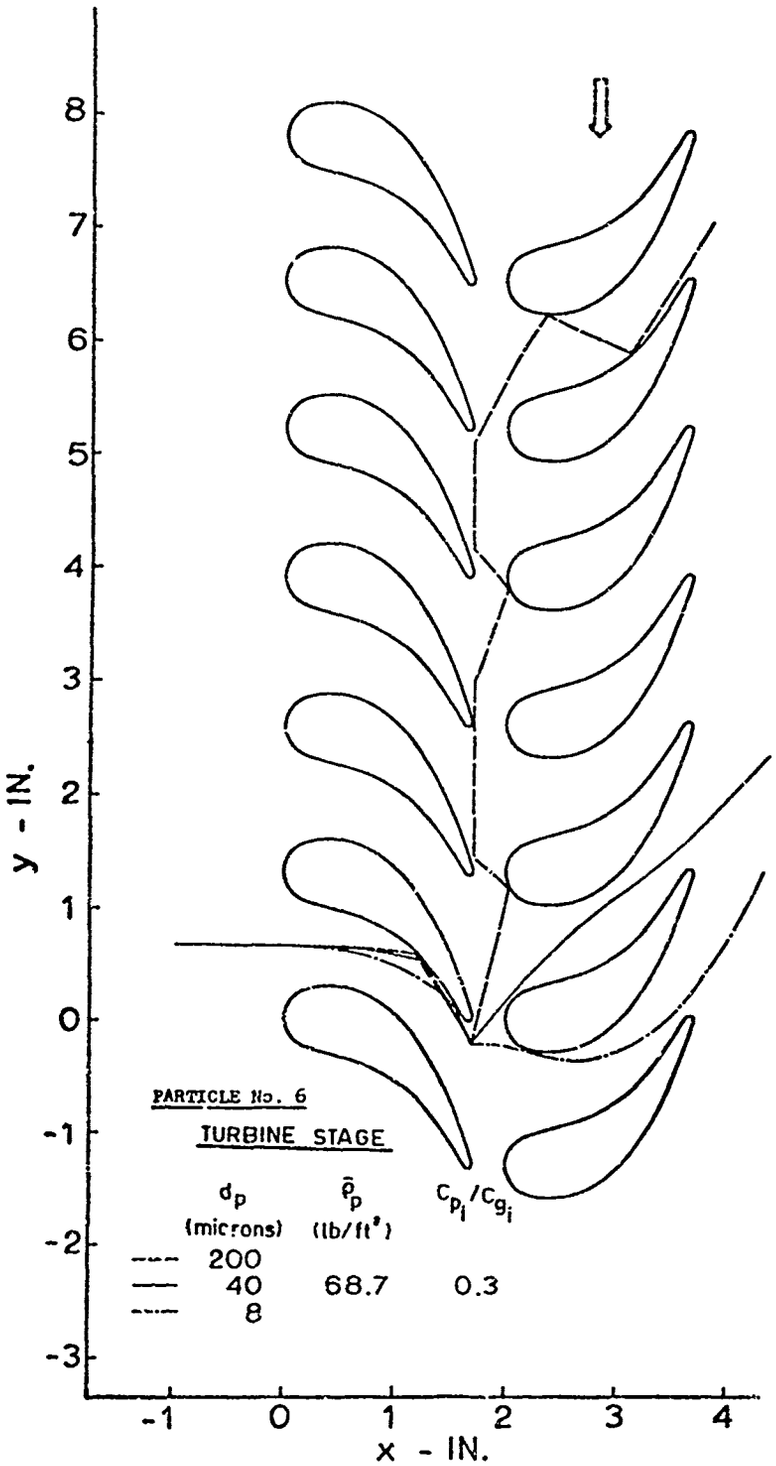

FIGURE 33 AXIAL AND TANGENTIAL COMPONENTS OF PARTICLE TRAJECTORIES RELATIVE TO THE ROTOR BLADES (EFFECT OF d_p)

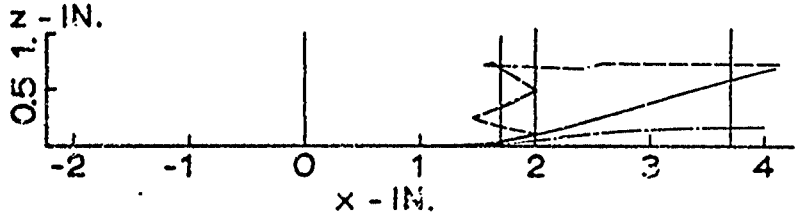

FIGURE 34 AXIAL AND RADIAL COMPONENTS OF PARTICLE TRAJECTORIES

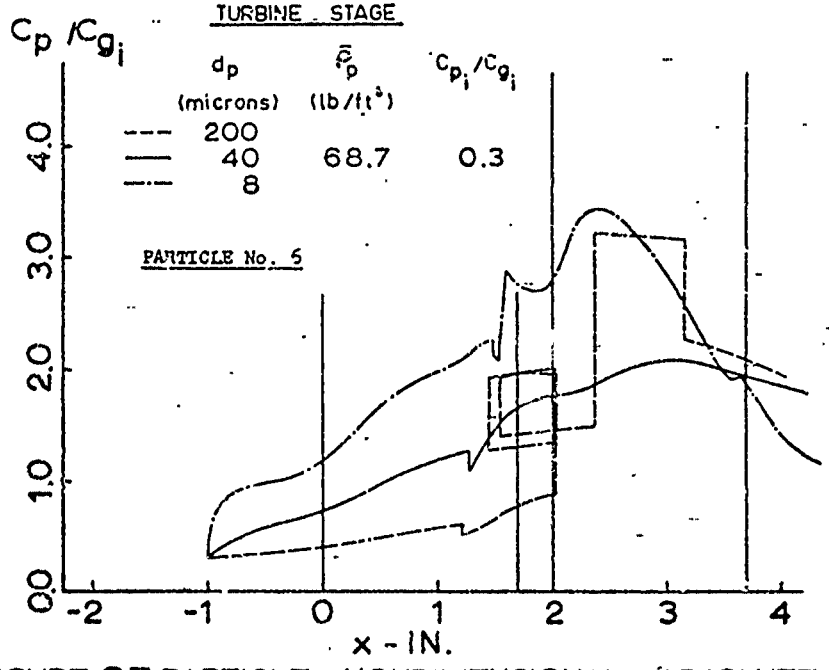

FIGURE 35 PARTICLE NONDIMENSIONAL ABSOLUTE VELOCITIES. (EFFECT OF d_p)

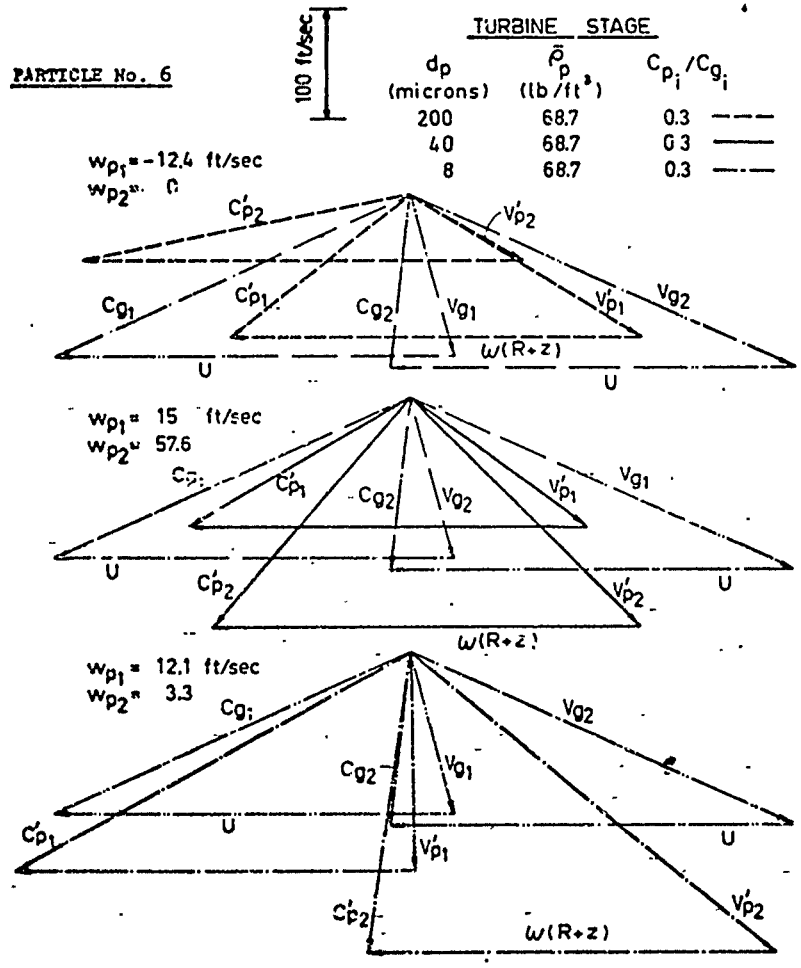

FIGURE 36 PARTICLE VELOCITY DIAGRAM

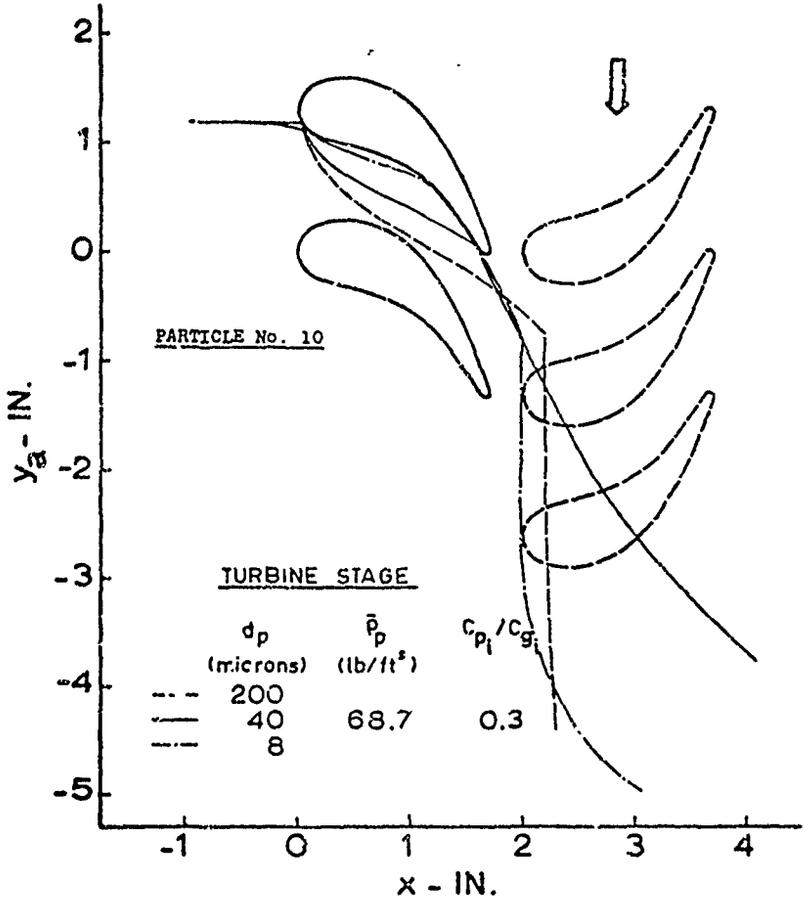

FIGURE 37 AXIAL AND TANGENTIAL COMPONENTS OF PARTICLE TRAJECTORIES (EFFECT OF d_p)

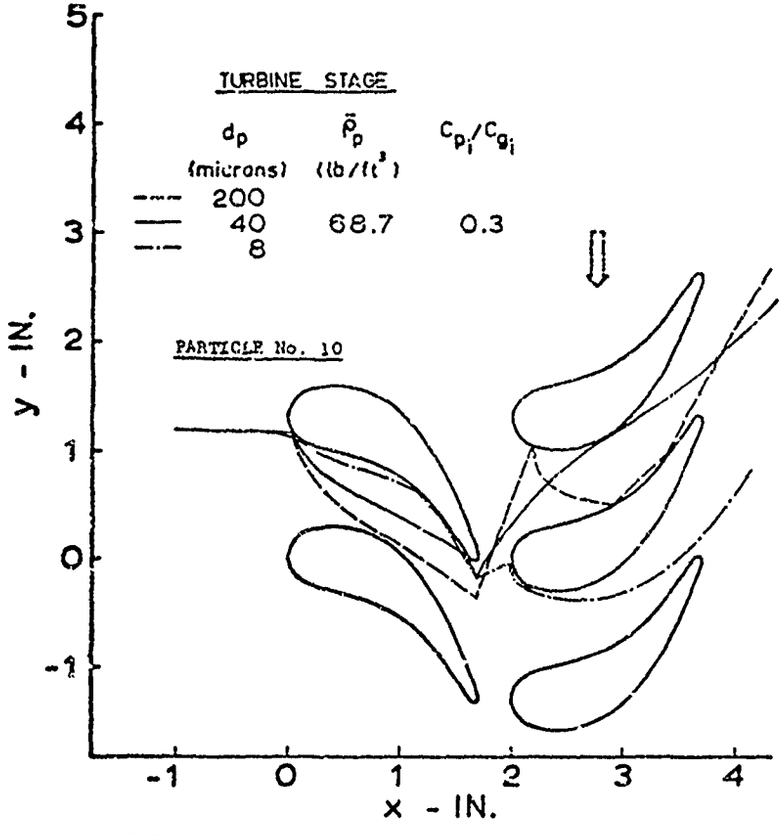

FIGURE 38 AXIAL AND TANGENTIAL COMPONENTS OF PARTICLE TRAJECTORIES RELATIVE TO THE ROTOR BLADES (EFFECT OF d_p)

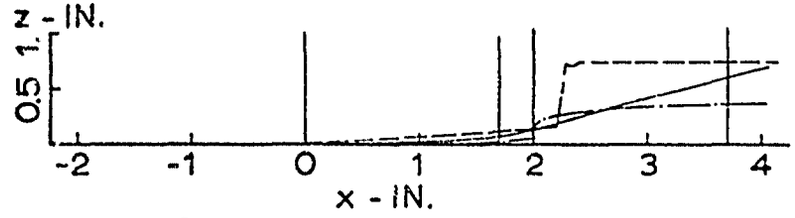

FIGURE 39 AXIAL AND RADIAL COMPONENTS OF PARTICLE TRAJECTORIES

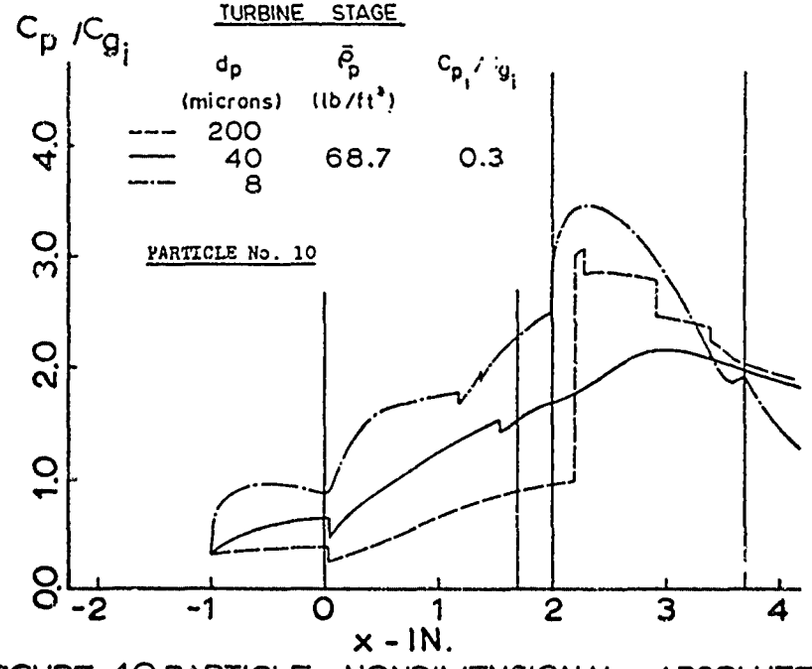

FIGURE 40 PARTICLE NONDIMENSIONAL ABSOLUTE VELOCITIES (EFFECT OF d_p)

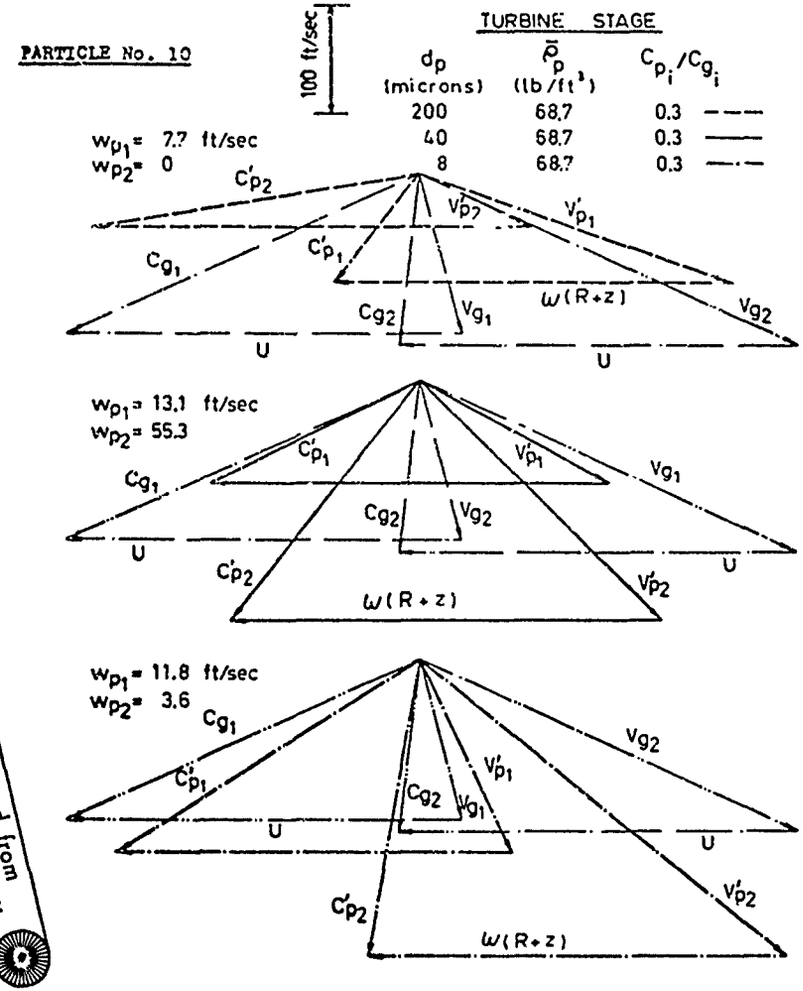

FIGURE 41 PARTICLE VELOCITY DIAGRAM

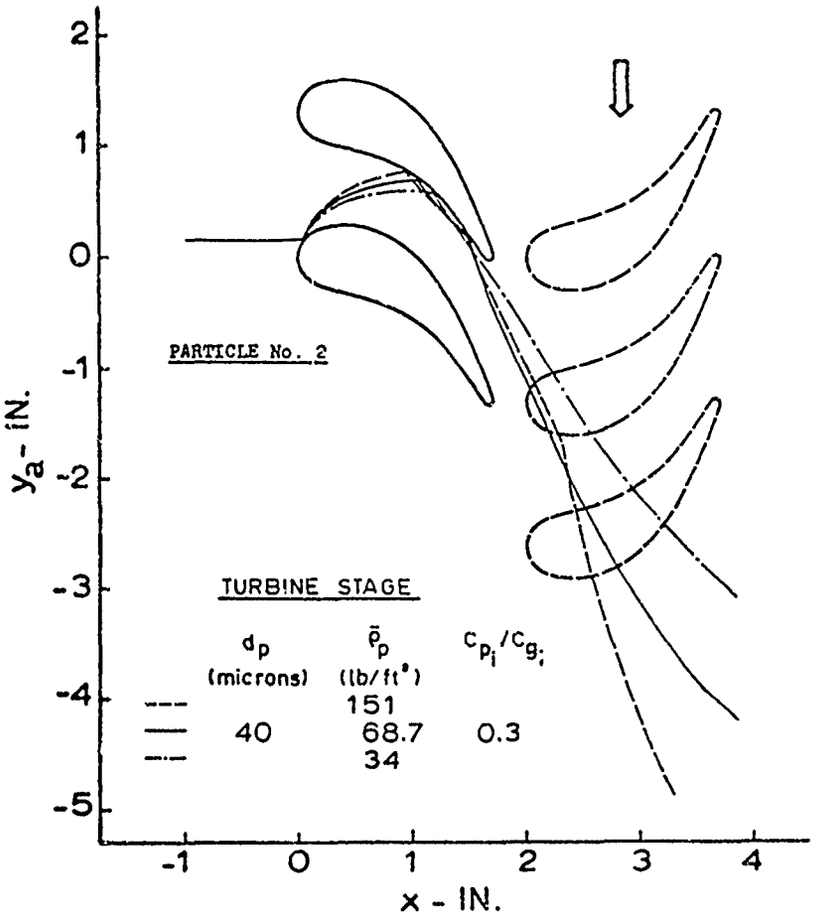

FIGURE 42 AXIAL AND TANGENTIAL COMPONENTS OF PARTICLE TRAJECTORIES (EFFECT OF $\bar{\rho}_p$)

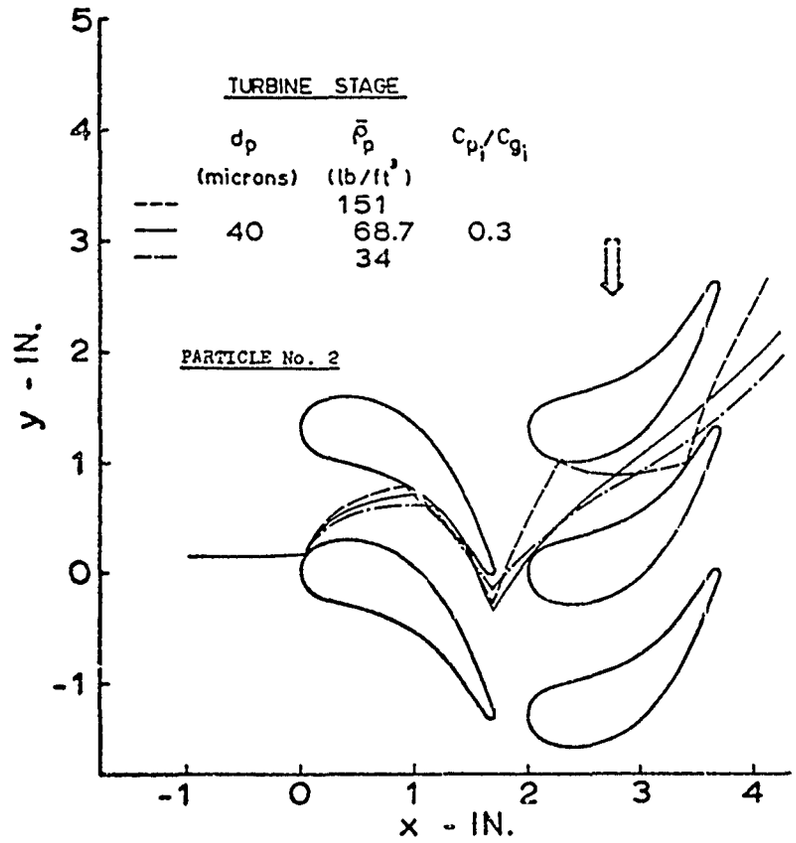

FIGURE 43 AXIAL AND TANGENTIAL COMPONENTS OF PARTICLE TRAJECTORIES RELATIVE TO THE ROTOR BLADES (EFFECT OF $\bar{\rho}_p$)

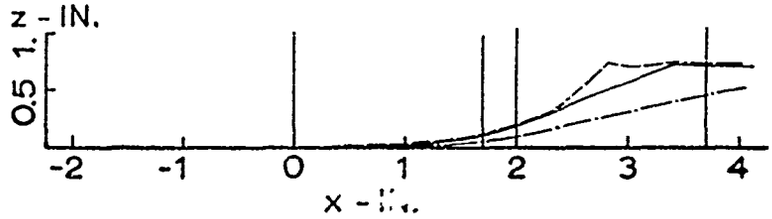

FIGURE 44 AXIAL AND RADIAL COMPONENTS OF PARTICLE TRAJECTORIES

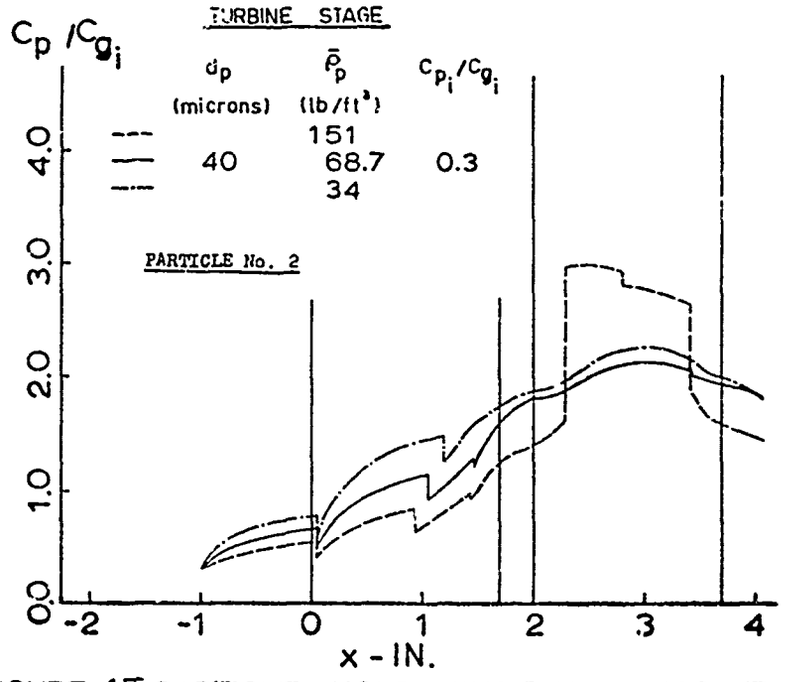

FIGURE 45 PARTICLE NONDIMENSIONAL ABSOLUTE VELOCITIES (EFFECT OF $\bar{\rho}_p$)

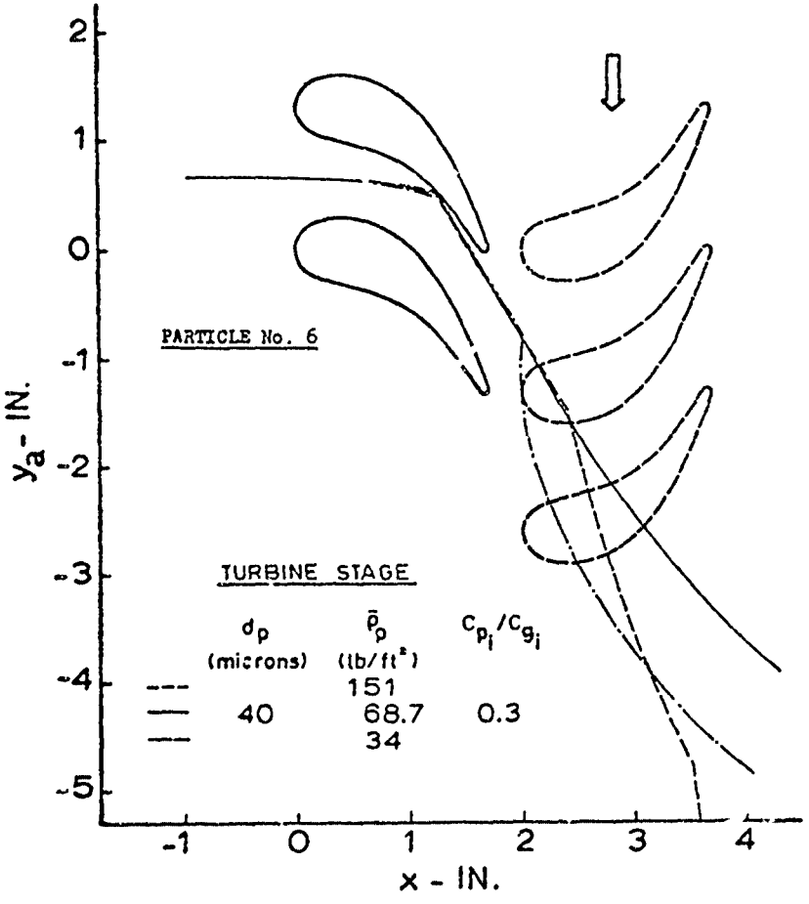

FIGURE 46 AXIAL AND TANGENTIAL COMPONENTS OF PARTICLE TRAJECTORIES (EFFECT OF $\bar{\rho}_p$)

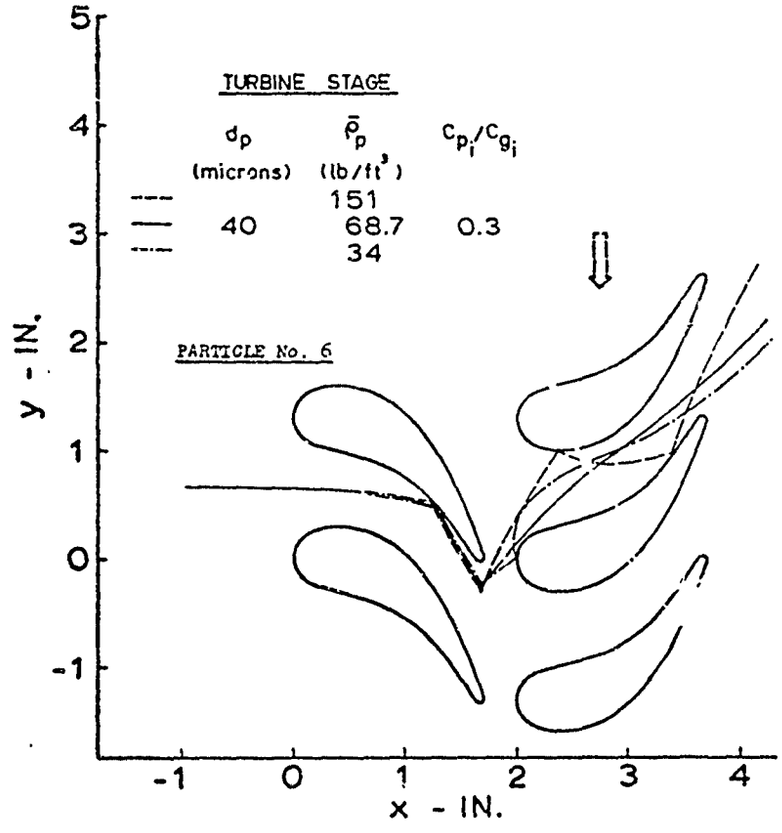

FIGURE 47 AXIAL AND TANGENTIAL COMPONENTS OF PARTICLE TRAJECTORIES RELATIVE TO THE ROTOR BLADES (EFFECT OF $\bar{\rho}_p$)

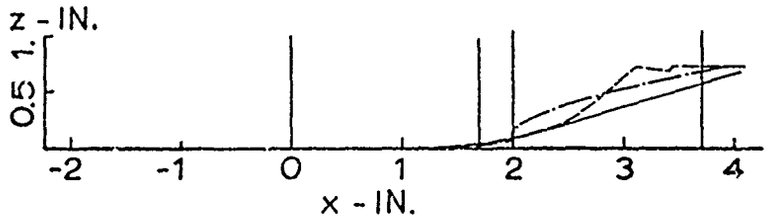

FIGURE 48 AXIAL AND RADIAL COMPONENTS OF PARTICLE TRAJECTORIES

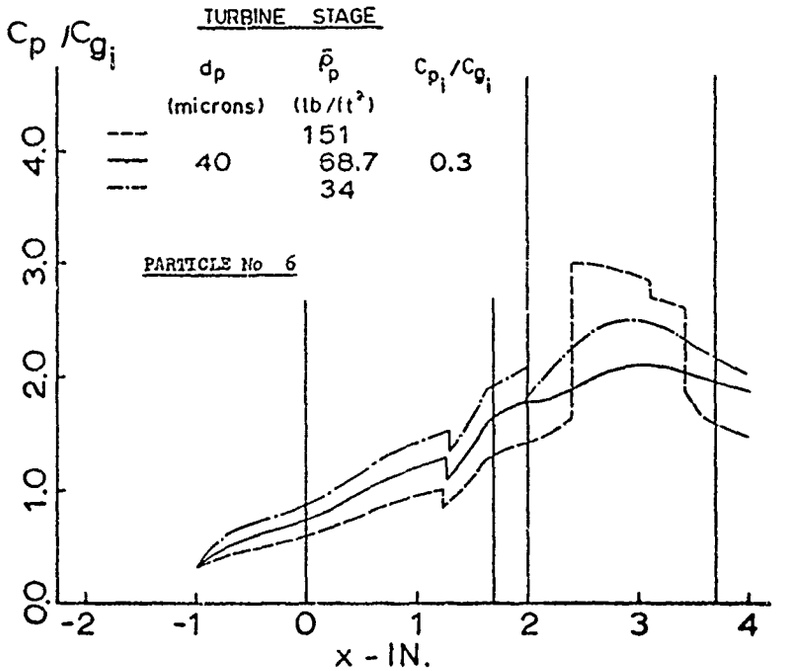

FIGURE 49 PARTICLE NONDIMENSIONAL ABSOLUTE VELOCITIES (EFFECT OF $\bar{\rho}_p$)

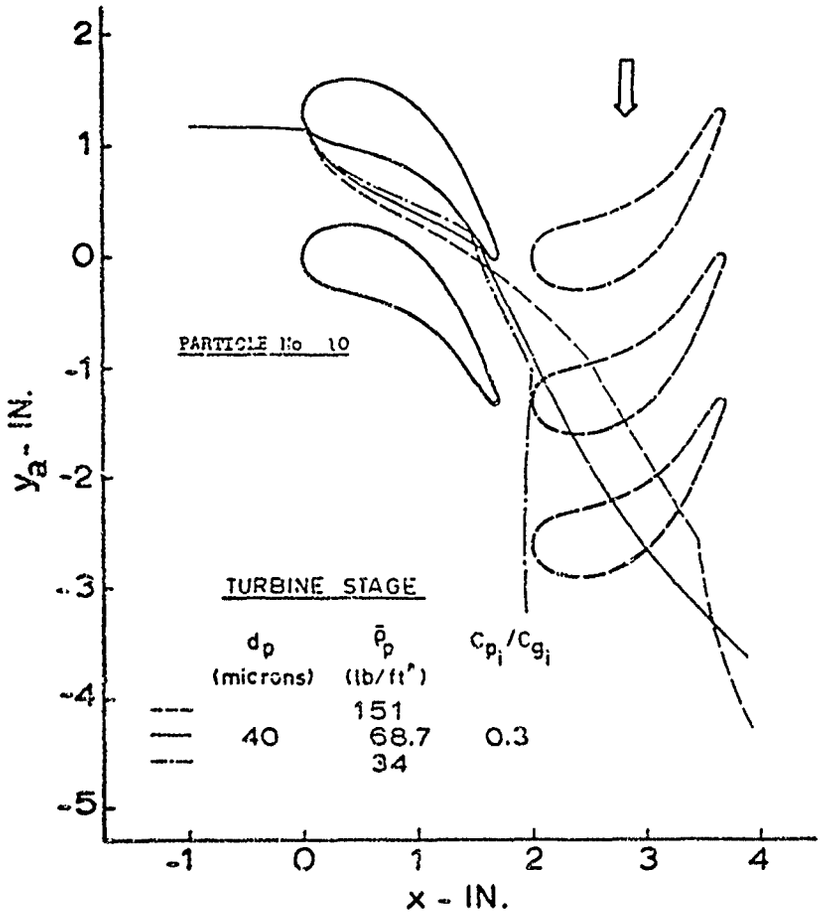

FIGURE 50 AXIAL AND TANGENTIAL COMPONENTS OF PARTICLE TRAJECTORIES (EFFECT OF $\bar{\rho}_p$)

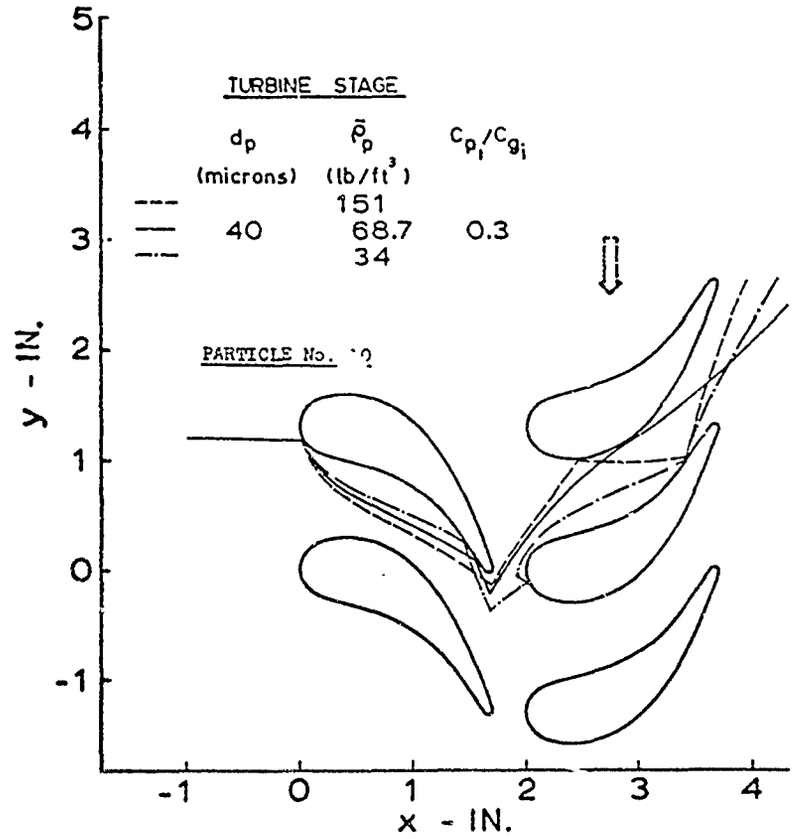

FIGURE 51 AXIAL AND TANGENTIAL COMPONENTS OF PARTICLE TRAJECTORIES RELATIVE TO THE ROTOR BLADES (EFFECT OF $\bar{\rho}_p$)

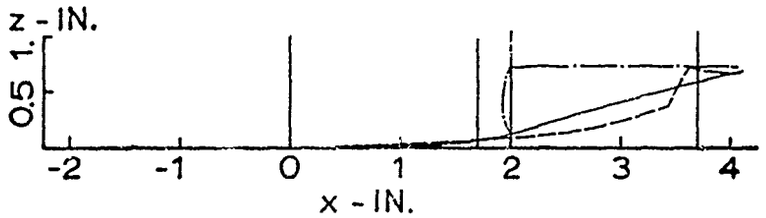

FIGURE 52 AXIAL AND RADIAL COMPONENTS OF PARTICLE TRAJECTORIES

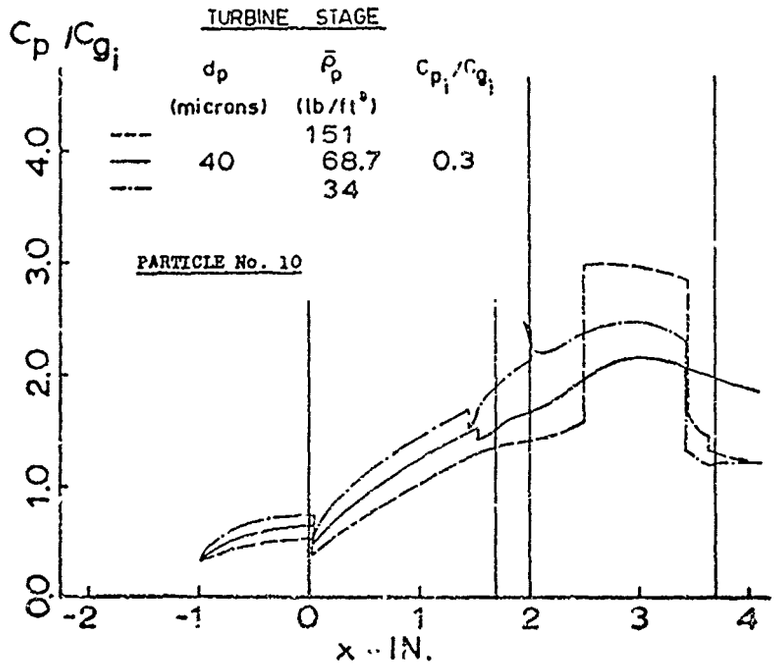

FIGURE 53 PARTICLE NONDIMENSIONAL ABSOLUTE VELOCITIES (EFFECT OF $\bar{\rho}_p$)

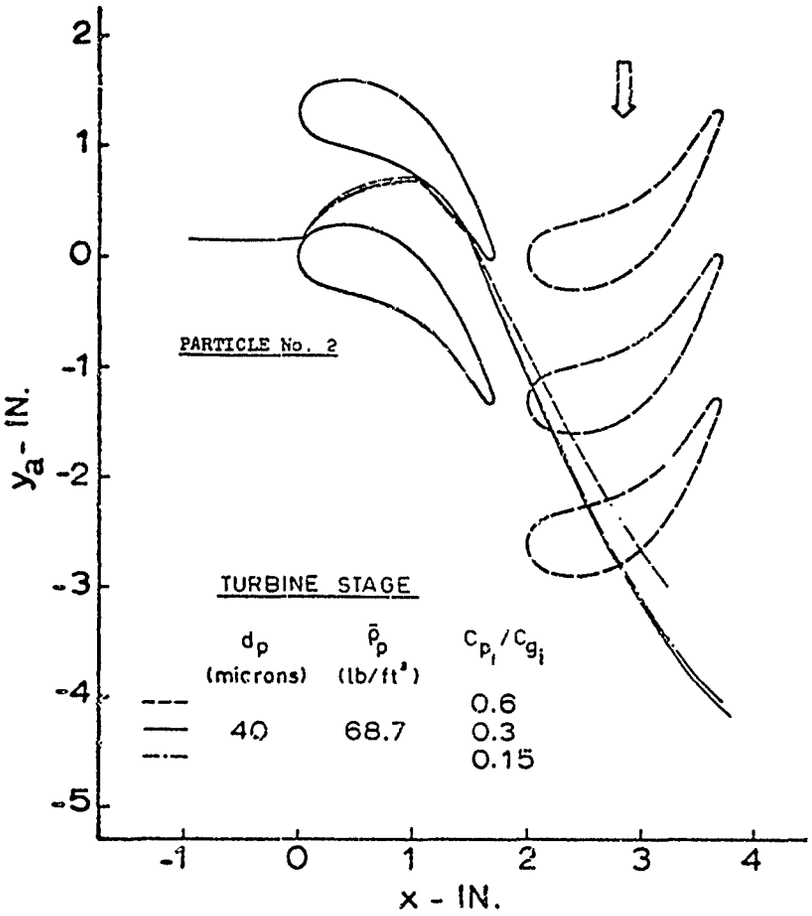

FIGURE 54 AXIAL AND TANGENTIAL COMPONENTS OF PARTICLE TRAJECTORIES (EFFECT OF C_{p_i}/C_{g_i})

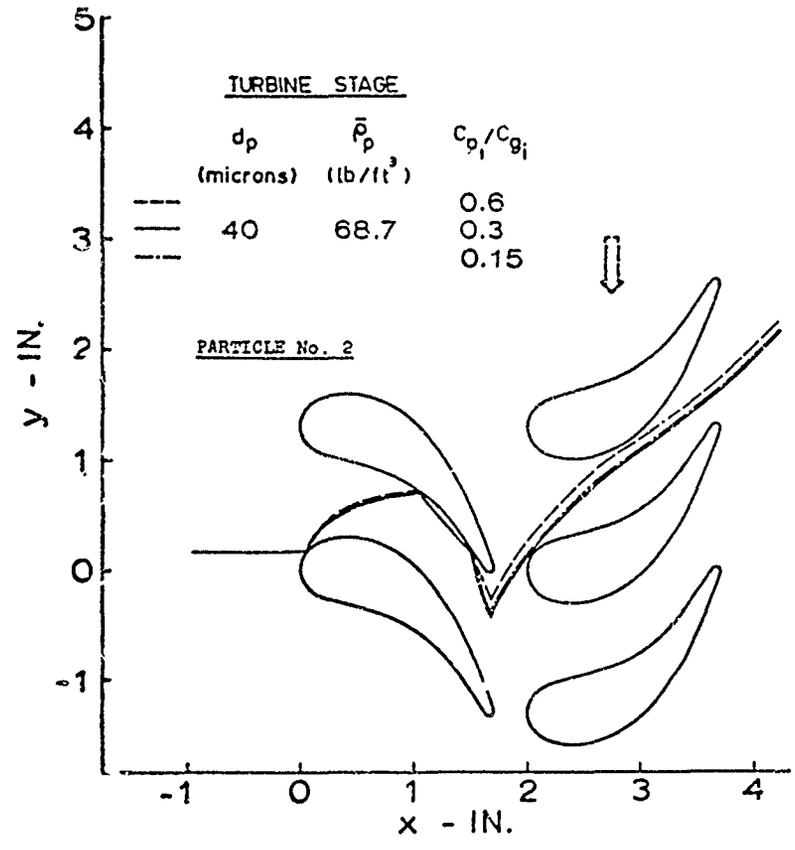

FIGURE 55 AXIAL AND TANGENTIAL COMPONENTS OF PARTICLE TRAJECTORIES RELATIVE TO THE ROTOR BLADES (EFFECT OF C_{p_i}/C_{g_i})

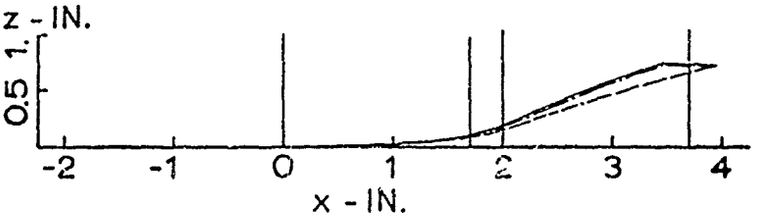

FIGURE 56 AXIAL AND RADIAL COMPONENTS OF PARTICLE TRAJECTORIES

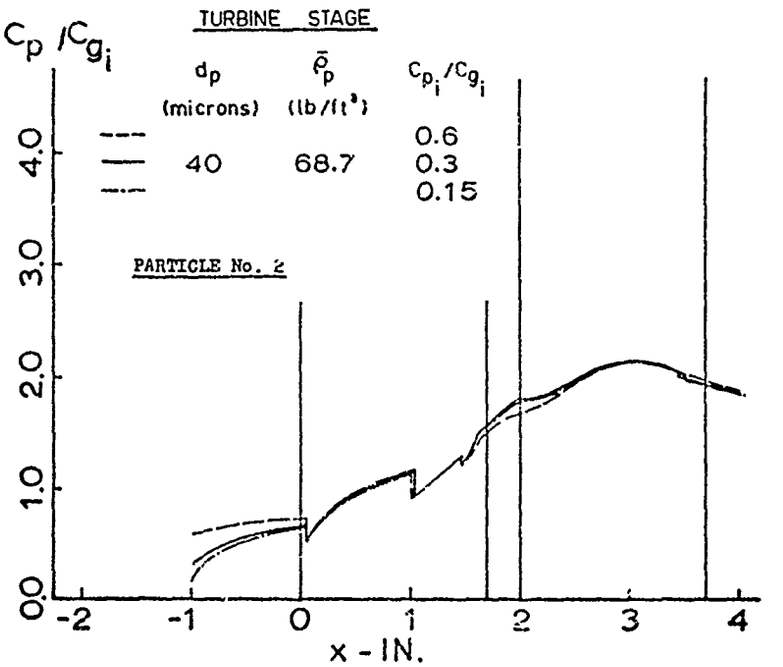

FIGURE 57 PARTICLE NONDIMENSIONAL ABSOLUTE VELOCITIES (EFFECT OF C_{p_i}/C_{g_i})

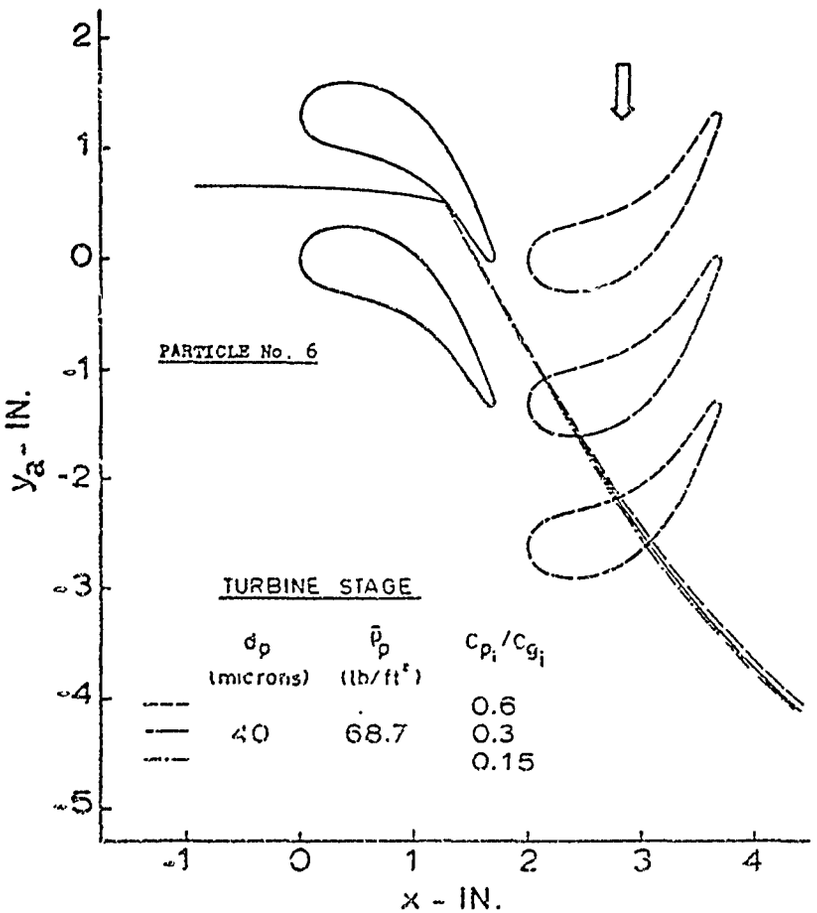

FIGURE 58 AXIAL AND TANGENTIAL COMPONENTS OF PARTICLE TRAJECTORIES (EFFECT OF C_{p_i}/C_{g_i})

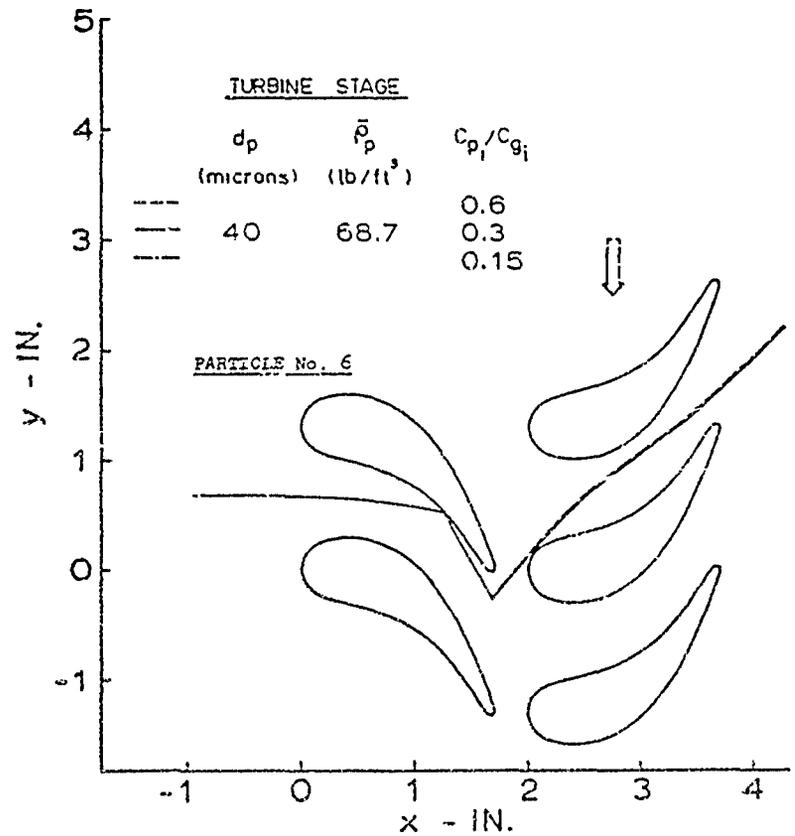

FIGURE 59 AXIAL AND TANGENTIAL COMPONENTS OF PARTICLE TRAJECTORIES RELATIVE TO THE ROTOR BLADES (EFFECT OF C_{p_i}/C_{g_i})

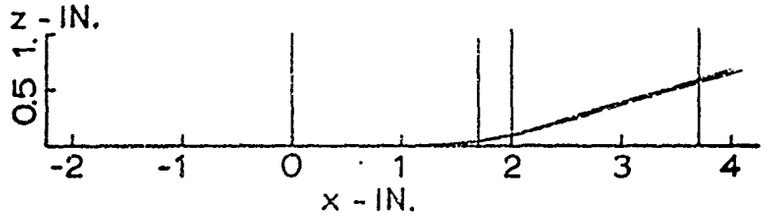

FIGURE 60 AXIAL AND RADIAL COMPONENTS OF PARTICLE TRAJECTORIES

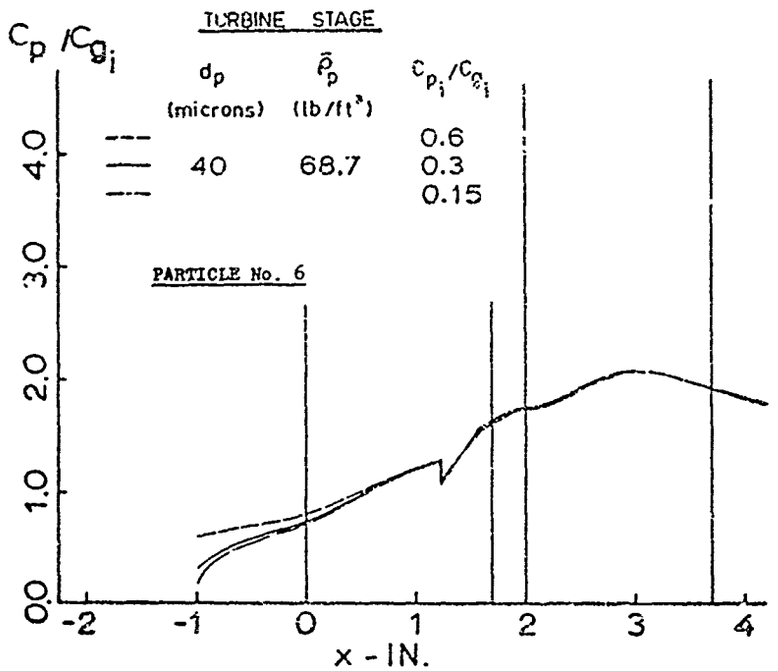

FIGURE 61 PARTICLE NONDIMENSIONAL ABSOLUTE VELOCITIES (EFFECT OF C_{p_i}/C_{g_i})

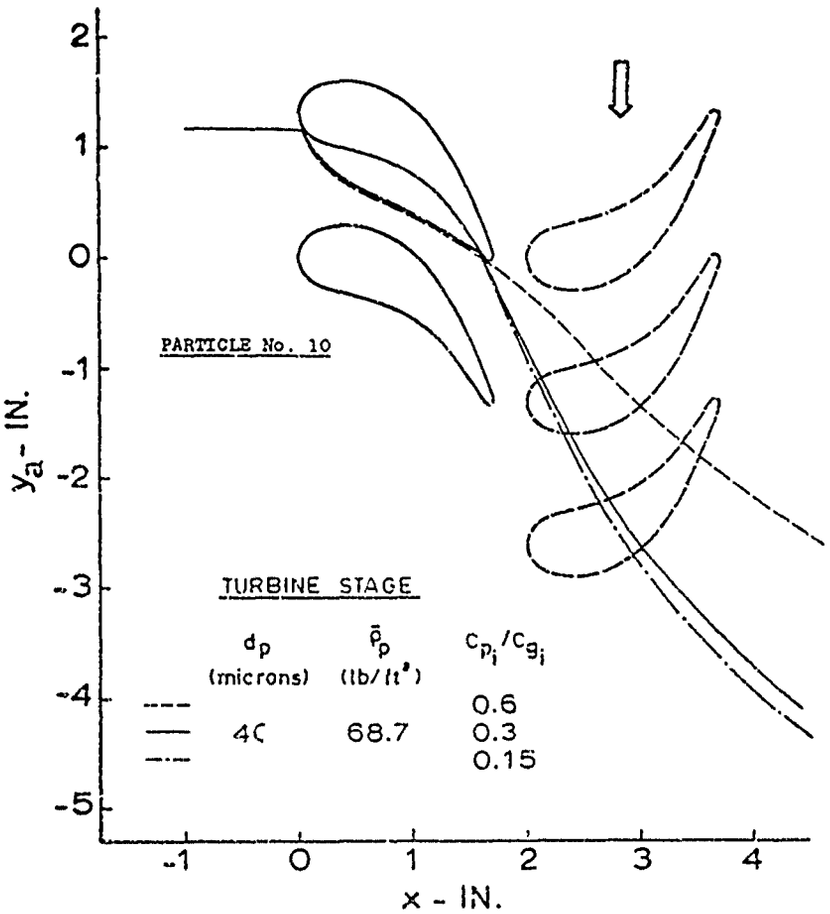

FIGURE 62 AXIAL AND TANGENTIAL COMPONENTS OF PARTICLE TRAJECTORIES (EFFECT OF C_{p_i}/C_{g_i})

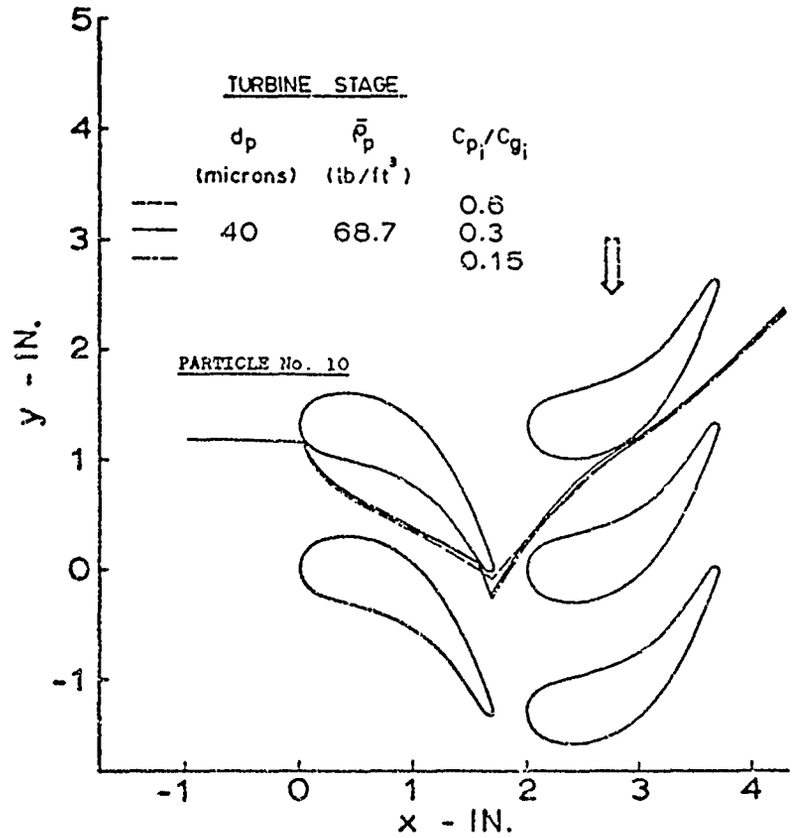

FIGURE 63 AXIAL AND TANGENTIAL COMPONENTS OF PARTICLE TRAJECTORIES RELATIVE TO THE ROTOR BLADES (EFFECT OF C_{p_i}/C_{g_i})

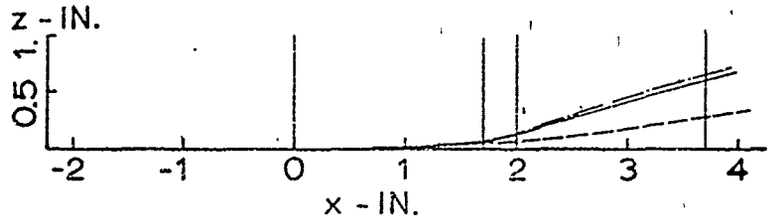

FIGURE 64 AXIAL AND RADIAL COMPONENTS OF PARTICLE TRAJECTORIES

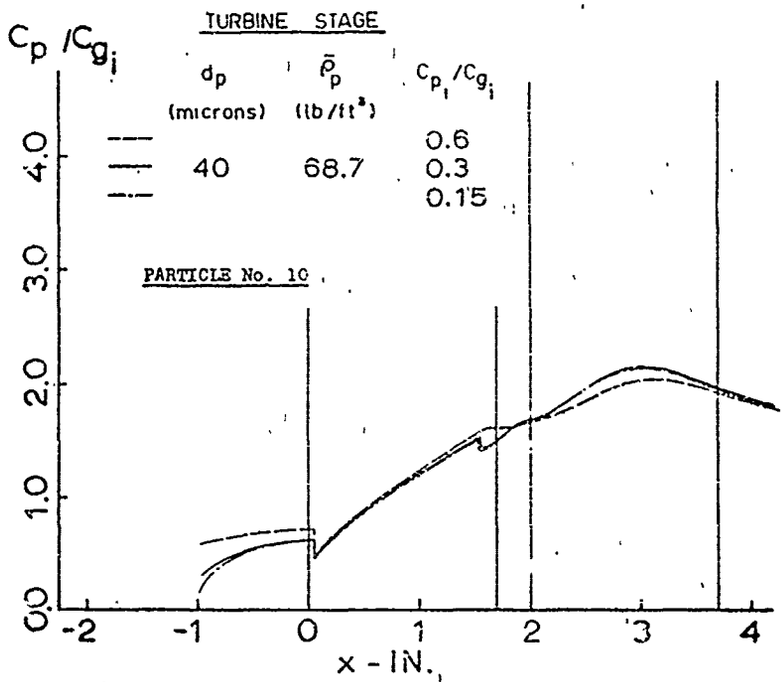

FIGURE 65 PARTICLE NONDIMENSIONAL ABSOLUTE VELOCITIES (EFFECT OF C_{p_i}/C_{g_i})